Heliyon 10 (2024) e38174

Contents lists available at ScienceDirect

Heliyon

journal homepage: www.cell.com/heliyon

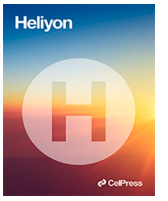

Review article

Dual-locked fluorescent probes for precise diagnosis and targeted treatment of tumors

Tang Gao [a,1], Can Xiang [b,1], Xintao Ding [c], Mingxing Xie [a,*]

[a] Department of Ultrasound Medicine, Union Hospital, Tongji Medical College, Huazhong University of Science and Technology, Wuhan, 430022, China
[b] Department of Scientific Management, Union Hospital, Tongji Medical College of Huazhong University of Science and Technology, Wuhan, 430022, China
[c] Department of Biomedical Informatics, Columbia University Graduate School of Arts and Sciences, New York, NY, United States

ARTICLE INFO

Keywords:
Fluorescent probes
Dual-stimuli responsive
Tumor imaging
Tumor treatment

ABSTRACT

Cancer continues to pose a significant threat to global health, with its high mortality rates largely attributable to delayed diagnosis and non-specific treatments. Early and accurate diagnosis is crucial, yet it remains challenging due to the subtle and often undetectable early molecular changes. Traditional single-target fluorescent probes often fail to accurately identify cancer cells, relying solely on single biomarkers and consequently leading to high rates of false positives and inadequate specificity. In contrast, dual-locked fluorescent probes represent a breakthrough, designed to enhance diagnostic precision. By requiring the simultaneous presence of two specific tumor-associated biomarkers or microenvironmental conditions, these probes significantly reduce non-specific activations typical of conventional single-analyte probes. This review discusses the structural designs, response mechanisms, and biological applications of dual-locked probes, highlighting their potential in tumor imaging and treatment. Importantly, the review addresses the challenges, and perspectives in this field, offering a comprehensive look at the current state and future potential of dual-locked fluorescent probes in oncology.

1. Introduction

Cancer is often associated with high mortality rates and stands as the second leading cause of death globally [1]. This primarily stems from delays in detection and diagnosis, which cause many patients to miss the critical period for effective treatment [2,3]. This high mortality rate significantly impacts global health [4]. However, studies have shown that early detection of cancer at the cellular/molecular level can greatly enhance treatment outcomes. For instance, data from the National Cancer Control Center of the Australian Cancer Council indicate a stark contrast in survival rates based on the stage at which breast cancer is diagnosed: a 100 % one-year survival rate for Stage 1 compared to 69 % for Stage 4 [5]. Thus, improving the accuracy of early cancer diagnosis is crucial. One of the primary challenges in cancer diagnosis is the difficulty in distinguishing cancerous cells from normal ones, especially when no clear pathological structural changes are evident. However, certain cellular alterations-like increased enzyme expression and variations in pH and viscosity-are indicative of cancer [6,7]. Therefore, there is a pressing need to develop technologies capable of

* Corresponding author.
E-mail address: xiemx@hust.edu.cn (M. Xie).
[1] Contributed equally to this work.

https://doi.org/10.1016/j.heliyon.2024.e38174
Received 2 July 2024; Received in revised form 18 September 2024; Accepted 19 September 2024
Available online 19 September 2024

accurately identifying these molecular differences, which are crucial for precise diagnosis and subsequent therapeutic interventions.

In this context, Fluorescence imaging using fluorescent probes has emerged as a powerful tool in cancer imaging, offering non-invasiveness, speed, sensitivity, high selectivity, and real-time capabilities [8–10]. The customizable nature of fluorescent probes allows for flexible design to suit different detection environments and targets, catering to diverse detection needs [11]. Recent research efforts have been focused on developing fluorescent probes that target specific biomarkers and microenvironments unique to cancer cells, such as enzymes, reactive oxygen species (ROS), pH levels, viscosity, and hypoxia [12–16]. These targeted probes are not only pivotal for precise cancer diagnosis but also hold immense potential in precision therapy [12,17,18]. By accumulating selectively within tumor tissues or targeting specific molecular entities, these probes facilitate localized and precise drug delivery, enhance the efficacy of optical-guided surgical resections and photodynamic therapy, and thereby improve patient outcomes [19].

Despite their advancements, single-analyte-activated probes face challenges, such as the risk of "false-positive" signals and limitations in detecting interconnected biomarkers or molecular events crucial to tumor progression [20]. Furthermore, single-locked probes are incapable of detecting two interconnected biomarkers or molecular events at targeted or diseased sites. While co-administering two distinct single-locked probes could potentially allow for the simultaneous imaging of different biomarkers or events, variations in their penetration capabilities, pharmacokinetics, and metabolism can impact their performance and sensing accuracy in bioimaging applications. Dual-locked fluorescent probes, which respond to two distinct analytes, offer a solution by providing enhanced specificity and reducing the chances of false positives [21–23]. These dual-locked probes, whether featuring two responsive sites or a single unit that reacts to sequential analytes, represent a significant step forward in overcoming the limitations of single-lock probes. By enabling the simultaneous imaging of multiple tumor-related biomarkers or the controlled release of therapeutic agents, dual-locked probes facilitate a deeper understanding of tumor biology and improve the precision of both diagnosis and treatment [24,25].

This review has outlined the progress in the field of dual-lock probes, focusing on their structural design, response mechanisms, and biological applications. We have delved into various design strategies and highlighted key examples where dual-lock probes have been instrumental in tumor imaging and treatment (Scheme 1). As we look to the future, addressing the unresolved challenges and harnessing the full potential of dual-lock probes will be crucial in advancing the field of cancer diagnostics and therapeutics, offering new avenues for precision medicine and improving patient outcomes.

2. Dual-locked probes for tumor imaging

The early diagnosis of tumors is challenging due to the subtle cellular and molecular changes that often go unnoticed. This lack of early symptoms can lead patients to ignore potential signs of tumors. Sensitive detection of tumor biomarkers is pivotal in early cancer diagnosis and significantly enhances patient prognosis [26]. Proteases, which are overexpressed in many tumors, are promising diagnostic and therapeutic targets due to their key role in cancer progression [27]. However, relying on a single overexpressed protease for tumor detection can lead to false positives, which undermines diagnostic accuracy. In this context, the simultaneous detection of multiple biomarkers with dual-locked probes offers a new pathway to improve early cancer detection's precision and specificity [28–30]. These probes are engineered to respond to two distinct cellular or molecular events in tumor cells, enhancing early-stage tumor detection accuracy. By pinpointing specific biomarker combinations or environmental conditions unique to cancerous cells,

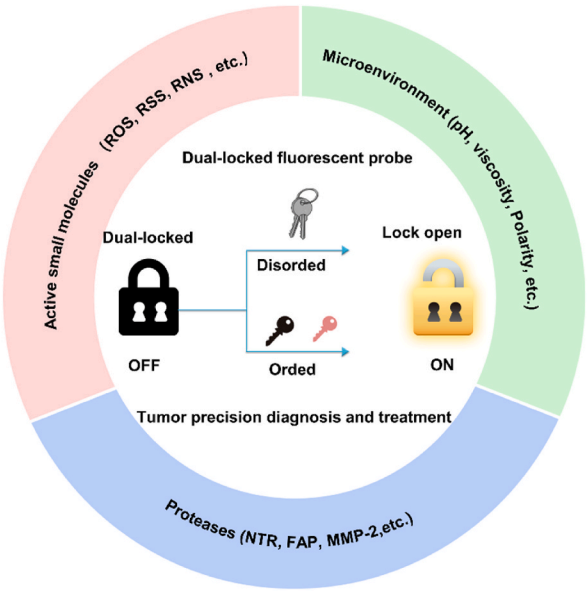

Scheme 1. Diagram of a dual-locked fluorescent probe for tumor diagnosis and treatment, highlighting its activation mechanism.

dual-locked probes refine the identification of malignancies, aiding in better patient prognosis and treatment outcomes. The choice of biomarkers is crucial in designing dual-locked probes. Enzymatic markers like matrix metalloproteinases (MMPs) and bioactive small molecules, along with tumor microenvironment parameters like hypoxia and pH, are key to the probes' design. These elements ensure the probes' precise activation and targeting within the tumor microenvironment, improving tumor imaging's specificity and sensitivity.

2.1. Sequentially activated dual-locked probes for tumor imaging

Sequentially activated probes are designed to emit signals only when they encounter two specific analytes in a predetermined order. This section highlights dual-locked probes that utilize a single optical channel for a stepwise response, showcasing their application in tumor imaging. (Fig. 1a).

2.1.1. Sequentially activated by tumor microenvironment

The tumor microenvironment is notably marked by hypoxia, characterized by reduced oxygen levels. This condition boosts glucose metabolism and leads to the accumulation of acidic substances like lactic acid and carbonic acid, consequently increasing the proton (H^+) concentration and creating an acidic environment within the tumor [31]. This acidic environment is closely associated with tumor progression and poor prognosis. Leveraging hypoxia as a biomarker is therefore instrumental for the early detection of tumors, with the acidity serving as an additional metric to differentiate between healthy and cancerous tissues [7,32]. Jiang et al. introduced a cutting-edge deep near-infrared (NIR) nanoprobe **1**, engineered to activate in response to both acidity and hypoxia, facilitating the early identification of cancerous growths [33]. This nanoprobe features an oxygen-sensitive core that emits in the deep NIR spectrum and is encased in an acid-cleavable PEG shell. This design ensures stability and discreetness in circulation, with the PEG shell serving as a trigger for the NIR signal under acidic conditions. (Fig. 1b). After intravenous injection of nanoprobe **1** (50 mg·kg−1 of body weight), the phosphorescence signal of nanoprobe **1** was exclusively co-localized with the bioluminescence signal from orthotopic tumors without any background signal, as observed 24 h post-injection (Fig. 2a). In the lung of mice, we detected the phosphorescence signal of nanoprobe **1** (Fig. 2b), which allowed for the detection of up to 33 nodules through phosphorescence imaging, compared to only 2 to 8 nodules visible to the naked eye (Fig. 2c). The dual response to the tumor's acidic and hypoxic environment, coupled with its deep NIR capability, allows for the sensitive detection of minute tumor formations or even early-stage metastatic lesions. The research highlights the nanoprobe's efficacy in discerning tumor hypoxia across various tumor types, underscoring its potential in refining cancer diagnosis and enhancing the accuracy of imaging hypoxic tumor regions, thus offering a new avenue for early cancer detection and more effective treatment strategies.

2.1.2. Sequentially activated by proteases

Enzymes linked to tumors play a significant role in cancer progression. The imaging of these enzymes' distribution and activity across varied spatial and temporal contexts is vital for precise diagnosis and the refinement of cancer treatments. Matrix metalloproteinases (MMPs), especially those within the extracellular matrix, are crucial in cancer progression through their role in degrading matrix proteins [34]. MMP-2, in particular, is instrumental in promoting tumor invasion and metastasis, establishing it as a critical marker for cancer detection and a target for specific therapeutic interventions [35]. Additionally, the role of intracellular caspase-3 as an early apoptosis indicator provides essential real-time data on cell death, pivotal for assessing treatment effectiveness and for the screening of apoptosis-related drugs [36]. Zhang and colleagues have developed a novel probe **2**, utilizing dual-FRET mechanism for the sequential detection of MMP-2 and caspase-3 [37]. Probe **2** comprises fluorophore-quencher pairs connected by peptides specific to the target enzymes (Fig. 1c). When the probe interacts with MMP-2 or caspase-3, the cleavage of peptide sequences occurs, separating the fluorophore-quencher pairs and enabling fluorescence recovery. This capability of sequential detection offers high sensitivity and selectivity in identifying MMP-2 and caspase-3 activities. The probe's efficacy is further validated through its response to the enzymes and their inhibitors, underscoring its specificity and sensitivity to these molecular targets. The probe's design facilitates real-time monitoring of cell apoptosis signals, rendering it a valuable tool for drug screening and the dynamic imaging of apoptosis processes.

The role of anticancer drugs primarily involves inducing apoptosis, hence monitoring the activation of the caspase cascade is fundamental in evaluating drug efficacy and in drug screening processes. Liu and colleagues have developed a fluorescent probe **TPETH-DVED-TPS** (Fig. 1d), which leverages aggregation-induced emission (AIE) properties for the real-time, multiplex imaging of caspase cascade activation [38]. This probe integrates two distinct AIE fluorogens, which exhibit unique emission spectra but are excitable at a unified wavelength, connected via a hydrophilic peptide substrate specific to caspase-8 and caspase-3. The sequential cleavage of the peptide substrate by caspase-8 and caspase-3 activates green and red fluorescence in sequence, enabling the dynamic observation of early apoptotic cell events. The application of this probe in conjunction with anticancer drugs like doxorubicin (DOX) and 5-fluorouracil (5-Fu) demonstrated distinct fluorescence patterns correlating with drug efficacy, showcasing the probe's potential in real-time therapeutic monitoring.

Cancer immunotherapy stands as a promising avenue enhancing patient survival rates across various cancer types [39,40]. However, it is essential to balance its therapeutic advantages against potential adverse effects, notably the immune-related adverse events (irAEs) that can be severe [41,42]. Therefore, assessing the effectiveness of cancer immunotherapy is crucial for optimizing treatment strategies and ensuring patient well-being. Pu and team introduced innovative approaches using advanced molecular optical probes for assessing the effectiveness of cancer immunotherapy. One such innovation is the Tandem-Locked Fluorescent NETosis Reporter **TNR1**, designed for the sensitive and specific detection of NETosis, a neutrophil activity relevant to cancer immunotherapy

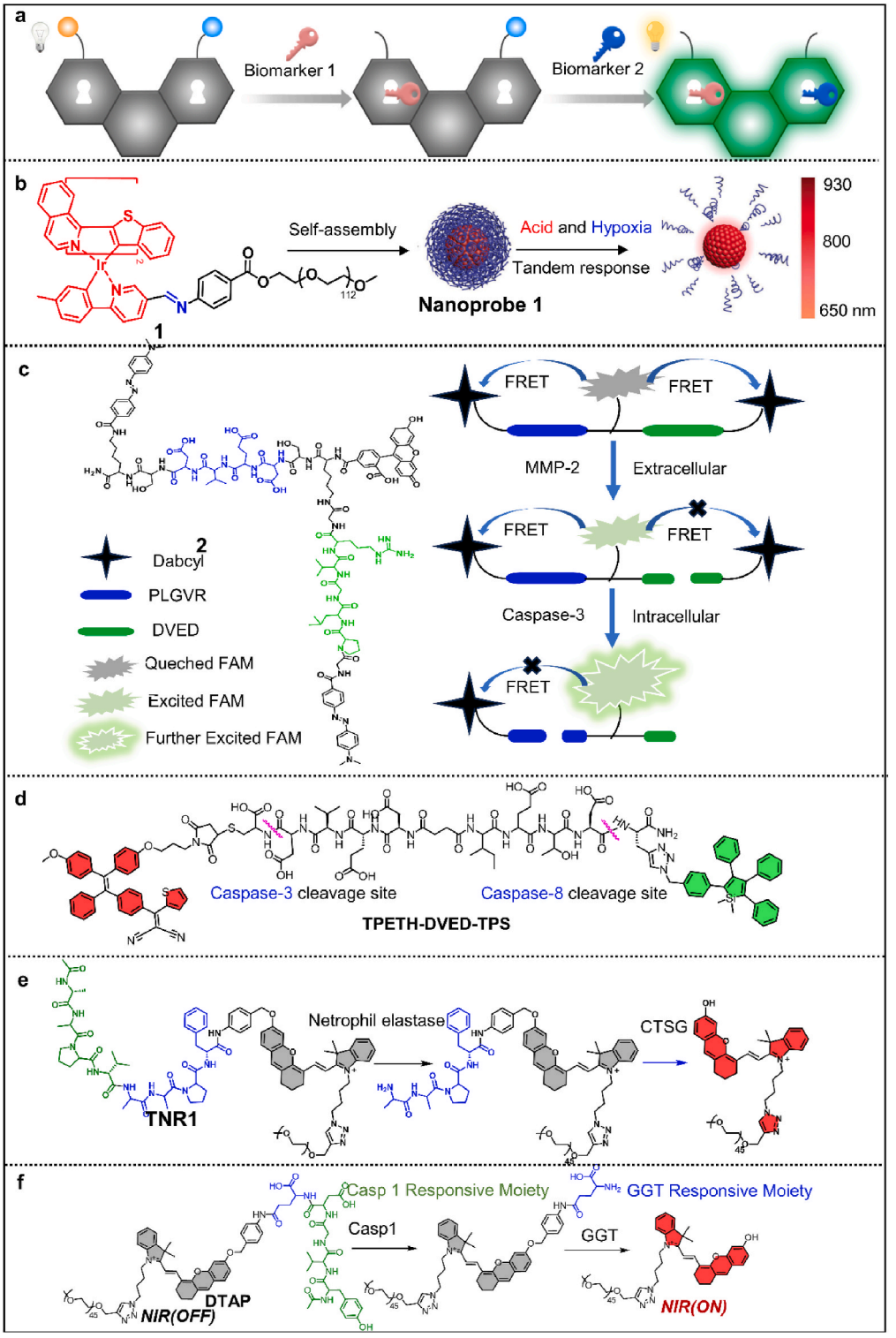

(caption on next page)

Fig. 1. Dual-lock probes with two reactive sites that initiate two successive reactions. (a) Illustration of a dual lock-and-key probe mechanism showing sequential activation where the probe requires successive interactions first with Biomarker 1 and then with Biomarker 2 to enable signal activation; (b) Structure of fluorescent probe **1** illustrating its self-assembly and response to acid and hypoxia. Reprinted from ref. 33 with permission by John Wiley and Sons and Copyright Clearance Center; (c) The chemical structure of probe 2 and its FRET-based mechanism enable the sequential detection of MMP-2 and caspase-3. Reprinted from ref. 37 with permission by Royal Society of Chemistry (d) Chemical structure of **TTPETH-DVED-TPS**, highlighting the caspase-3 and caspase-8 cleavage sites. (e) Structure of TNR1 and its sequential signal activation in response to neutrophil elastase and CTSG. (f) Chemical structures of **DTAP** and their sequential response to Casp1 and GGT.

[43]. **TNR1** distinguishes NETosis from neutrophil activation in live cell imaging through a tandem-locked design. The choice of peptide sequence within these tandem blocks critically influences the probe's specificity for detecting NETosis. For **TNR1**, the selected tandem peptide sequence, N-acetyl-Ala-Ala-Pro-Val/Ala-Ala-Pro-Phe (AAPV/AAPF), is designed to be sequentially cleaved by the enzymes NE and CTSG, enhancing its specificity (Fig. 1e). This sequential cleavage by NE and CTSG allows TNR1 to specifically emit near-infrared fluorescence (NIRF) signals with a 48-fold enhancement only in the presence of both NE and CTSG, providing high detection specificity for NETosis. After treatment, TNR1 was intravenously injected into living mice, and longitudinal NIRF imaging was performed for 48 h to quantify signals at the tumor site. In the NETosis inducer-treated group, the signal initially increased within the first 2 h but rapidly decreased thereafter, a pattern also observed in the NETosis reducer and saline control groups (Fig. 2d), likely due to rapid urinary excretion of activated TNR1. Quantification showed that tumor NIRF signals were 1.80 and 1.62 times higher in the NETosis inducer-treated group compared to the NETosis reducer and saline-treated groups, respectively (Fig. 2e). Immunofluorescence staining further confirmed that the expression of biomarkers (NE, CTSG) and NETosis markers (citH3, Ly6G) was reduced in mice undergoing immunotherapy compared to controls (Fig. 2f). The specificity of TNR1 in differentiating NETosis from other neutrophil activities offers a refined tool for monitoring and evaluating cancer immunotherapy, as demonstrated by its effectiveness in live cell imaging and in animal studies, providing valuable prognostic insights into treatment outcomes.

In their subsequent study, Pu et al. introduced a novel approach for real-time imaging of intratumoral pyroptosis in vivo using a molecular optical probe **DTAP** [44]. **DTAP** features a hemicyanine near-infrared fluorescence (NIRF) signaling unit, secured by two tandem-linked peptide sequences (Fig. 1f). These sequences are designed to be sequentially cleaved by caspase-1 (Casp1) and gamma-glutamyl transferase (GGT). Upon the occurrence of pyroptosis in cancer cells, the sequential action of Casp1 and GGT on DTAP triggers the activation of its NIRF signal, enabling dynamic imaging of cellular processes (Fig. 2g and **h**). This activation process allows for the specific detection of intratumoral pyroptosis, distinguishing it from other forms of cell death and normal tissue processes. After treatment, DTAP was injected into mice, and NIRF imaging showed a peak signal in tumors 4 h post-injection in those treated with the α-PD-L1/Cisp combination (Fig. 2i). To assess pyroptosis in the tumor immune microenvironment (TIM), ex vivo NIRF signals of DTAP were correlated with dendritic cell (DC) populations in TDLNs and tumor-infiltrating cytotoxic T lymphocytes during chemo-immunotherapy. Immunohistochemical analysis showed a 10.3-fold increase in DTAP signal with α-PD-L1/Cisp, 7.5-fold with Cisp alone, and 4.1-fold with α-PD-L1 alone, compared to controls (Fig. 2j). The probe's ability to passively accumulate in tumors and its specific reaction with Casp1 and GGT highlight its potential in accurately monitoring therapeutic responses and understanding pyroptosis's role in cancer treatment.

2.1.3. Sequentially activated by bioactive small molecules and proteases

In this section, we examine the integration of bioactive small molecules with protease-activated dual-locked probes, emphasizing their significant role in augmenting the precision of tumor imaging. These probes utilize the selective activation by specific proteases within the tumor microenvironment, coupled with the regulatory functions of bioactive molecules, to facilitate targeted imaging. In the realm of melanoma diagnostics, tyrosinase (TYR) is identified as a crucial biomarker due to its integral role in melanin synthesis [45]. While TYR exists in normal melanocytes, the advent of a dual-biomarker-activated fluorescent probe, utilizing the heightened levels of hydrogen peroxide (H_2O_2) in melanoma cells, bolsters the specificity of melanoma detection [46]. A notable advancement is the contribution by Huang et al., who developed a probe, **MB-m-borate** (Fig. 3a), for the precise detection of melanoma [47]. This probe employs a dual-locked strategy, amalgamating a borate group and a 3-hydroxybenzyloxy group as triggers, to enable specific activation by H_2O_2 and TYR. Such activation catalyzes the production of a fluorophore, MB, emitting near-infrared (NIR) fluorescence, ideal for bioimaging. This strategy assures activation solely in the presence of both triggers, specific to melanoma cells, diminishing the potential for false positives or elevated background signals seen with single biomarker-activated probes. Thus, this dual-locked approach enhances diagnostic precision and accuracy, heralding a promising method for developing new diagnostic tools for a variety of diseases, including melanoma. Building on this dual-locked strategy, Safacan Kolemen et al. developed a dual-locked fluorescent probe **RHT** (Fig. 3b), selectively imaging melanoma cells by responding to hydrogen sulfide(H_2S) and tyrosinase [48]. The probe's design, incorporating a resorufin core and a dinitrobenzene-phenolic masking unit, allows sequential activation by H_2S and TYR, providing selective melanoma cell imaging. Its high selectivity, reduced signal crosstalk, and improved spatial resolution position it as a valuable tool for early and precise cancer detection. Further research is imperative to assess RHT's clinical viability and address any potential limitations in clinical contexts.

Furthermore, Zhao et al. prepared **BOD-Py-PA** (Fig. 3c), a dual-biomarker responsive probe tailored for precise cancer imaging [49]. This probe is activated by alkaline phosphatase (ALP) and hydrogen sulfide (H_2S), incorporating a charge-reversal mechanism to improve its sensitivity. It features a monochlorinated boron-dipyrromethene (BODIPY) unit, which responds to H_2S, and an L-Phenylalanine methyl ester linker with a phosphate cap for ALP recognition. In buffer solution, the probe organizes into a nanoprobe with an initially negative surface charge, restricting its optical response to H_2S until ALP-mediated dephosphorylation induces a charge reversal, thereby boosting its H_2S sensitivity. This design not only enhances the probe's specificity but also its ability to distinguish

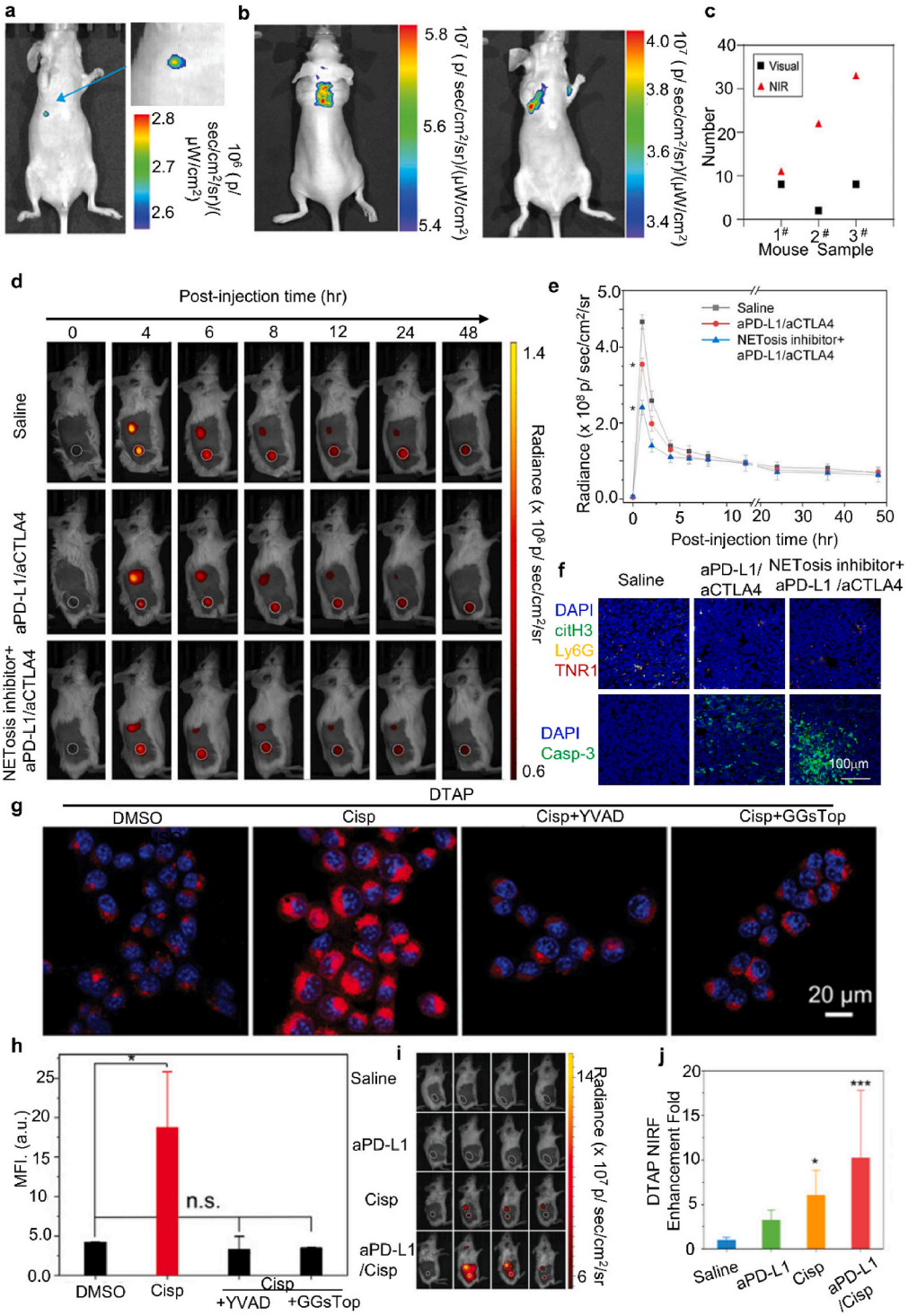

Fig. 2. (a) Whole-body NIR phosphorescence images of mice with orthotopically implanted small tumors at the breast site; (b) Whole-body NIR phosphorescence imaging of mice with lung metastases originating from primary MDA-MB-231 breast tumors following intravenous injection of nanoprobe **1**; (c) Number of metastatic nodules identified by both naked eye observation and NIR phosphorescence imaging in three different lung samples; (d) Representative NIRF images of live mice at various time points post-injection of **TNR1**in different treatment groups; (e) Dynamic NIRF intensity of tumors over time following **TNR1** injection in live mice from various treatment groups; (f) Representative confocal fluorescence microscopy images of tumor sections from mice after intravenous injection of **TNR1**; (g) Representative confocal fluorescence images of 4T1 cells incubated with **DTAP** following treatment with Cisp. From left to right: treated with vehicle (DMSO), Cisp (100 μM, 6 h), YVAD (Casp1 inhibitor Ac-YVAD-cmk, 60 μM, 1 h before and after Cisp treatment), or GGsTop (GGT inhibitor, 100 μM, 30 min post-Cisp treatment). Blue signal represents cell

nuclei stained with Hoechst 33342, while the red signal indicates activated **DTAP** or SAP; (h) Corresponding mean fluorescence intensity (MFI) of 4T1 cells; (i) Representative NIRF images of 4T1-tumor-bearing mice treated with or without chemo-immunotherapy after DTAP injection; (j) Ex vivo imaging of pyroptosis and evaluation of pyroptosis-enhanced anti-tumor immune responses in 4T1-tumor-bearing mice undergoing cancer therapy. Fold increase of **DTAP** NIRF signal is shown. All the above figures are reproduced with permission from references 33, 43, and 44, with authorization for citation.

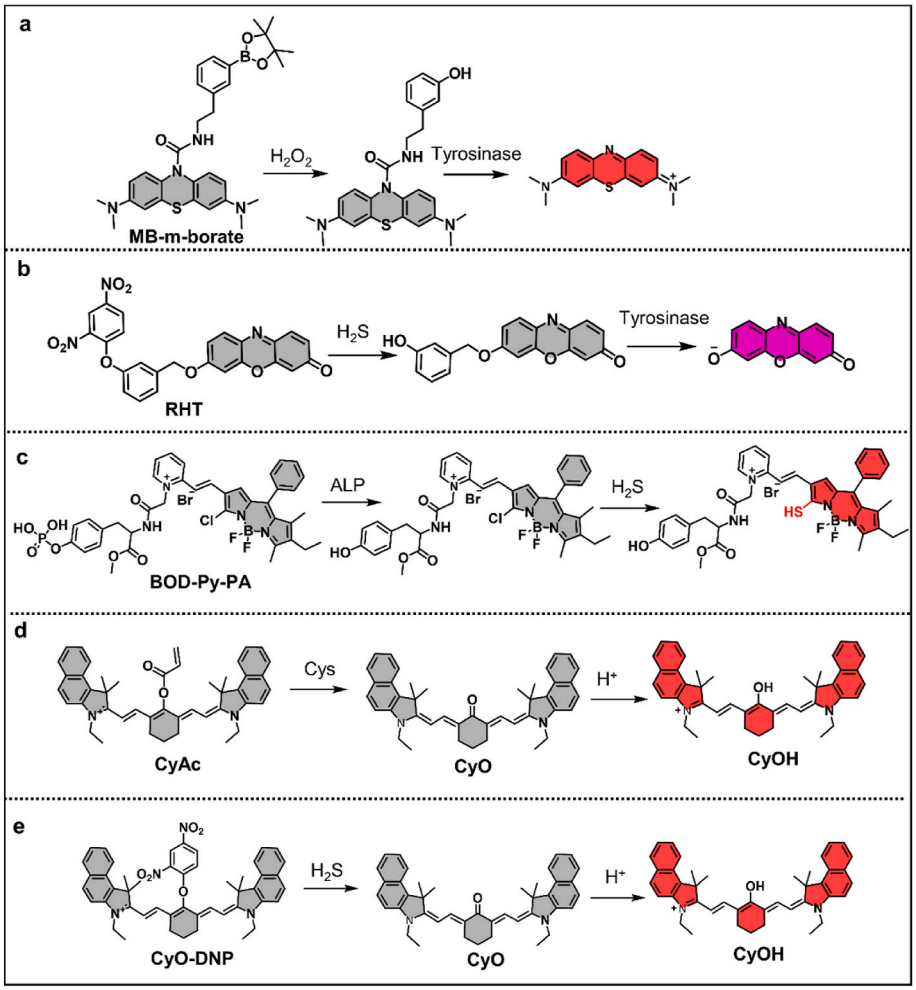

Fig. 3. Chemical structures and sensing mechanisms of probes designed for sequential activation by two specific biomarkers; (a) Transformation of **MB-m-borate** in the presence of H_2O_2 and subsequent activation by tyrosinase. (b) Molecular structure of **RHT** and its sequential activation with H_2S followed by tyrosinase. (c) Sequential activation of **BOD-Py-PA** by alkaline phosphatase (ALP) and H_2S; (d) Structural design of the CyAc probe to sequentially detect Cys and H^+. (e) Design of probe **CyO-DNP** for sequential detection of H_2S and H^+.

between cancerous and normal cells, as evidenced by an eightfold increase in fluorescence intensity in cancer cells compared to normal cells. Upon injection, **BOD-Py-PA** quickly produces visible fluorescent signals at tumor sites, highlighting its capability to effectively distinguish cancer cells and enhance the precision of in vivo cancer imaging.

2.1.4. Sequentially activated by bioactive small molecules and tumor microenvironment

In cancer biomarker research, cysteine (Cys) is recognized as a key indicator, with its concentration significantly elevated in tumor tissues compared to adjacent ones [50]. The lowered intracellular pH levels in malignant tumors, a phenomenon stemming from aerobic glycolysis known as the Warburg effect, establish pH as another pivotal biomarker [31,51]. Additionally, the overexpression of hydrogen sulfide (H_2S) in various cancer cells, notably in colon cancer cells via enhanced cystathionine-beta-synthase (CBS) activity, highlights H_2S's potential as a biomarker [52]. Given that single biomarkers may not provide sufficient diagnostic accuracy, developing a multiparametric analytical method capable of simultaneously detecting Cys, H_2S, and pH is vital for enhancing the precision of early cancer diagnosis. This integrated biomarker analysis strategy opens new avenues for early cancer detection and treatment.

Li et al. developed a near-infrared fluorescent probe, **CyAc**, as depictedin Fig. 3d, tailored for the sequential detection of cysteine

and H^+ [53]. The probe incorporates a cyanine fluorophore and an acrylate recognition group. In the presence of cysteine (Cys), **CyAc** converts to **CyO**, emitting a robust fluorescence signal at 660 nm. Subsequent pH reduction triggers H^+ to protonate **CyO** to **CyOH**, yielding fluorescence at 790 nm. Distinctively, **CyAc** can discern exogenous Cys in cells without interference from prevalent glutathione (GSH) and detect H^+ in living cells, with fluorescence intensifying as pH decreases. This probe differentiates between normal and cancer cells and has proven effective in mouse in vivo studies. Its sequential detection mechanism ensures reliability in complex

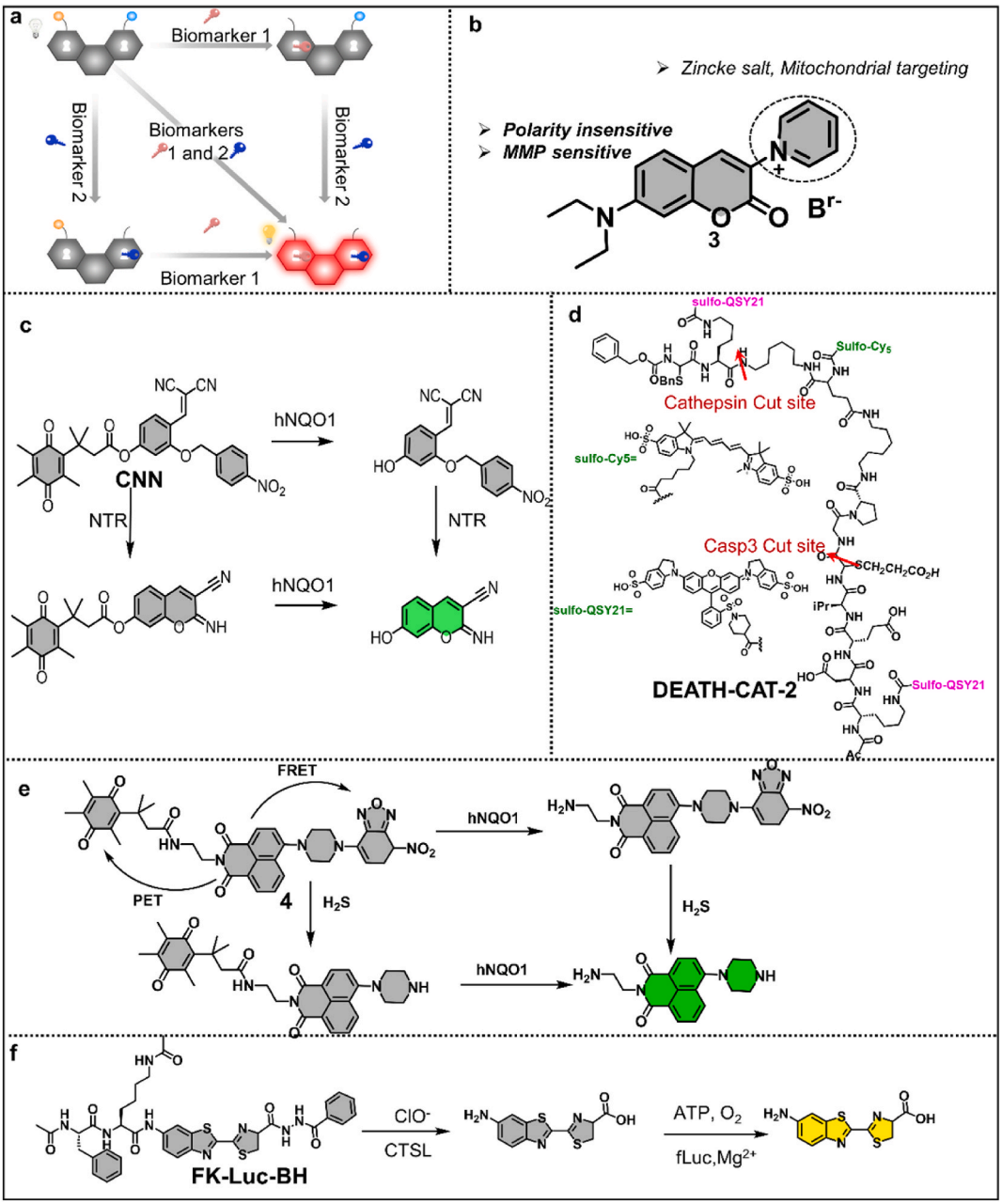

Fig. 4. AND-logic gate Dual-lock fluorescent probes. (a) AND-logic gate Dual-lock probes that are activated only when two analytes are present simultaneously. The activation of the probe signal is not affected by the order of analyte responses; (b) Structure of probe **3**, featuring a Zincke salt with mitochondrial targeting capabilities. This probe generates fluorescence signals ("ON") only under conditions of high pH (>7.0) and low polarity; (c) Structure of the probe **CNN** and its potential reaction mechanisms for NTR and hNQO1 detection, illustrating the transformation from the initial form to activated forms; (d) Structure of the probe **DEATH-CAT-2**, detailing the catalytic cleavage sites for caspase-3 and cathepsin; (e) Structure and activation mechanism of the AND-logic gate probe 4 based on FRET, showing the fluorescence signal activation in response to both hNQO1 and H_2S; (f) Activation mechanism of the FK-Luc-BH probe by CTS-L enzyme and ClO^- resulting in ATP and oxygen-dependent luminescence.

biological settings, positioning **CyAc** as a valuable asset for early cancer diagnosis. Expanding on this work, they created **CyO-DNP**, a near-infrared probe designed for the sequential detection of H_2S and H^+ in cancer cells [54]. This probe features a heptamethine dye as the fluorophore and a 2,4-dinitrophenyl (DNP) as the recognition group (Fig. 3e). In the presence of H_2S, **CyO-DNP** converts into **CyO**, producing intense fluorescence at 663 nm. This fluorescence is further enhanced to 793 nm following protonation by H^+. Such sequential detection capabilities make **CyO-DNP** a precise tool for fluorescence-based cancer diagnostics, targeting two critical biomarkers.

2.2. AND-logic gate probes for tumor imaging

AND-logic gate probes, compared to their single-analyte counterparts, offer significant advantages in tumor imaging. These include generating a pronounced "turn-on" fluorescence response by removing dual-locking groups and providing insights into the interplay between two analytes. Such probes necessitate the concurrent presence of two analytes for fluorescence activation, where a reaction at a single site yields minimal response (Fig. 4a). There are primarily two design strategies for these probes: converting pro-fluorophores into active fluorophores and constructing a fluorophore scaffold internally activated by dual analytes.

2.2.1. AND-logic gate probes activated by tumor microenvironment

In the context of tumor microenvironment, mitochondrial fluctuations are closely linked to cellular carcinogenesis. Mitochondria's essential function is to produce ATP via oxidative phosphorylation, providing the necessary energy for cellular functions [55]. This activity generates the mitochondrial transmembrane proton-motive force, which includes both the mitochondrial pH gradient and the mitochondrial membrane potential (MMP) [56]. In cancer cells, an elevated MMP is observed [57], resulting in an increased accumulation of delocalized lipophilic cations (DLCs) [58]. Individual parameters such as MMP, pH, and polarity may indicate cancer [59,60], combined assessment through an AND-logic gate substantially enhances the accuracy of cancer diagnosis [61,62]. Pursuing this integrated approach, Li et al. developed a novel fluorescent probe, referred to as Probe **3**, designed to improve cancer identification by leveraging these parameters within mitochondria [63]. This probe functions via the hydrolysis of a coumarin scaffold, producing fluorescence exclusively under conditions typical of cancerous mitochondria-low polarity, elevated pH, and high MMP. (Fig. 4b). The design incorporates a delocalized lipophilic cation (DLC) for its inherent mitochondrial targeting ability, responsive to variations in MMP. The differentiation in fluorescence between cancerous and non-cancerous cells hinges on the coumarin scaffold's hydrolysis, which is triggered only in the cancer cell mitochondria's unique environment. Utilizing 7-diethylamino coumarin for the fluorophore backbone and pyridine salts for mitochondrial targeting, the probe demonstrates heightened selectivity for cancer cell mitochondria, evidenced by its preferential activation in these cells (**Figre 5a**). When applied to cancer cells, probe **3** revealed a significant increase in fluorescence intensity-ranging from 6.7 to 51.9 times higher-compared to normal cells (Fig. 5b). This variability in fluorescence intensity across different cancer cell lines underscores the heterogeneity in their mitochondrial polarity and pH levels. Notably, the A549 cell line exhibited the most pronounced fluorescence signal, indicating the probe's specific activation in this context. In vivo imaging experiments further confirmed the probe's ability to accurately differentiate tumor tissues from normal tissues within complex organ structures, showcasing its potential as a highly specific tool for cancer detection.

2.2.2. AND-logic gate probes activated by proteases

In hypoxic tumor environments, nitroreductase (NTR) is recognized as a key marker of aggressiveness [64]. Similarly, the elevation of human NAD(P)H: quinone oxidoreductase isozyme I (hNQO1) across various cancers indicates a crucial link between enzyme levels and poor clinical outcomes, highlighting the importance of their early and accurate detection in cancer diagnostics [65]. Addressing this critical need, Tang et al. have developed a fluorescent probe, **CNN**, that simultaneously detects NTR and hNQO1 within living cells [66]. The probe employs an in-situ synthesis mechanism to produce a blue-emitting 7-hydroxy (2-imino) coumarin upon interaction (Fig. 4c). **CNN** features specific reactive moieties for NTR and hNQO1- a *p*-nitrobenzene group and a trimethyl-locked quinone propionic acid (Q3PA), respectively. In the absence of the target enzymes, fluorescence emission from CNN is suppressed by photoinduced electron transfer (PET) inhibition. however, enzyme presence triggers a cascade of reactions that generate a coumarin derivative, resulting in a significant fluorescence enhancement.

Building on the concept of selective enzyme detection in cancer diagnostics, Matthew Bogyo and his team have advanced this approach in the field of surgical oncology. They developed a AND-gate probe, **DEATH-CAT-2** (Fig. 4d), which is activated specifically by tumor-associated enzymes such as lysosomal cysteine cathepsins, executioner caspases, and fibroblast activation protein α [67]. This probe emits a fluorescence signal upon interaction with these enzymes, facilitating precise visualization of tumor margins during surgery. The enhanced fluorescence intensity of **DEATH-CAT-2** in tumor tissues, in comparison to negative controls and single-substrate probes, illustrates its utility in improving the selectivity and efficacy of optical contrast agents (Fig. 5c and **d**). Such advancements are pivotal in optimizing cancer removal, reducing recurrence rates, and preserving healthy tissue, thereby significantly enhancing patient outcomes in surgical oncology.

2.2.3. AND-logic gate probes activated by bioactive small molecules and the proteases

In the realm of precision oncology, the development of AND-logic gate probes that are dual-locked and responsive to both bioactive small molecules and proteases marks a substantial advancement. A noteworthy example is the work by Xi et al., who developed a dual-responsive fluorescent probe designed to detect hydrogen sulfide (H2S) and human NAD(P)H: quinone oxidoreductase isozyme 1 (hNQO1) simultaneously within living cells [68]. This probe, referred to as probe **4**, features two distinct chemoselective trigger groups that responsive to H_2S and hNQO1. (Fig. 4e). The activation of this probe requires the concurrent presence of both H_2S and hNQO1,

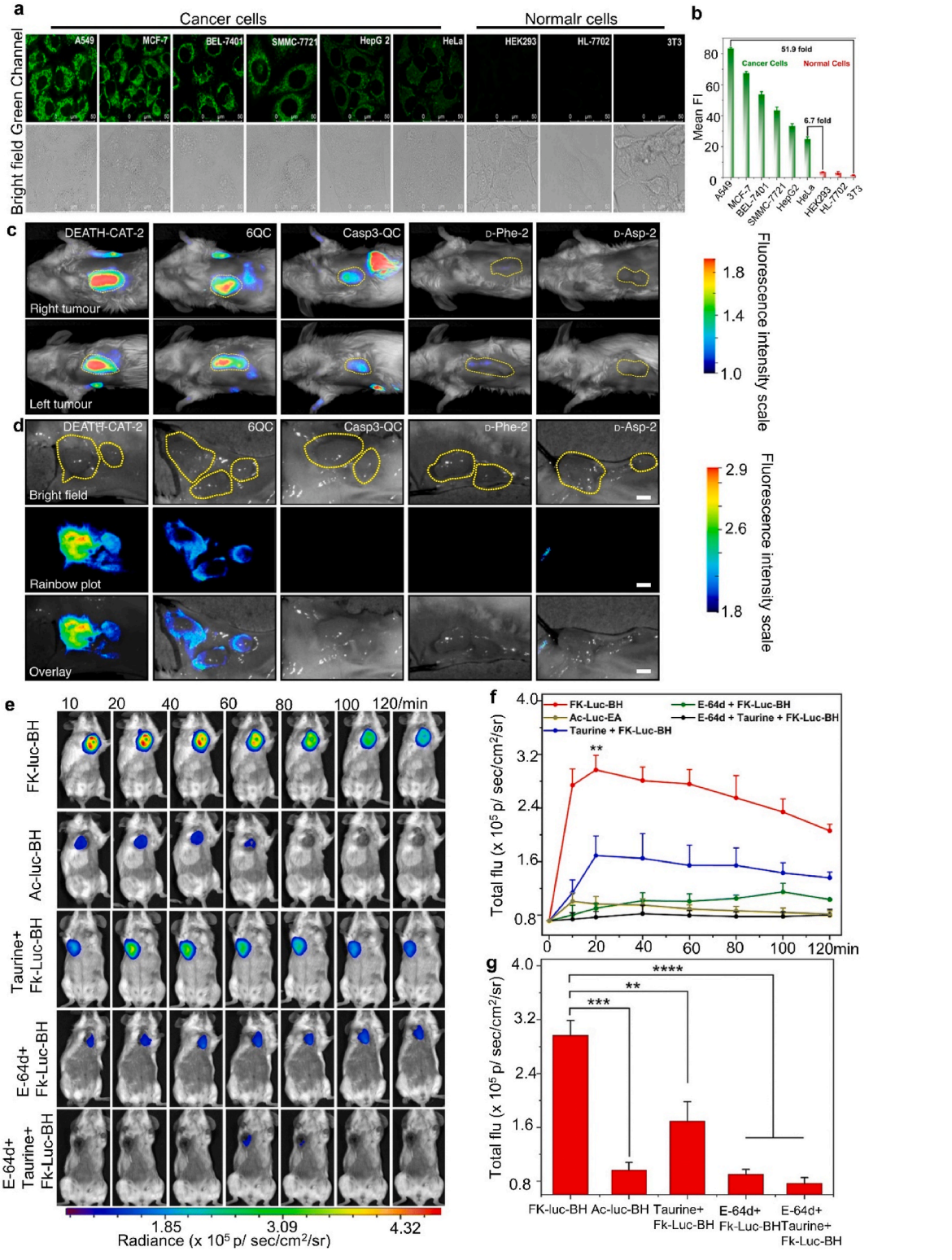

(caption on next page)

Fig. 5. (a) Confocal microscopy images of cancer and normal cells after incubation with probe 3 (10 μM) for 30 min. (b) Confocal microscopy images of cancer and normal cells following incubation with probe 3 (10 μM) for 30 min. (c) Imaging of live mice with 4T1 breast tumors, 2 h post-injection of the probe (20 nmol, intravenous). (d) Representative images of dissected 4T1 tumors, 2 h after probe injection. Tumor fluorescence in both live and dissected mice is displayed using rainbow plots and normalized for comparison across different groups. Fluorescence intensity scales on the right are expressed in arbitrary relative fluorescence units (RFU). Tumor outlines are indicated with yellow dotted lines. Scale bars, 3 mm. (e) Sequential in vivo bioluminescence imaging (BLI) of 4T1-fLuc tumor-bearing Balb/c mice following intraperitoneal administration of FK-Luc-BH at a dose of 12.5 mmol kg^{-1}. (f) Quantification of total photon emission using ImageJ software. (g) Quantified total photon output from (f) at 20 min. The above figures are reproduced with permission from references 63, 67, and 69, with authorization for citation.

leading to a fluorescence increase of over 400-fold, highlighting its remarkable sensitivity and specificity. The probe's effectiveness is demonstrated through its ability to distinguish between different cancer cell lines such as HT29 and HepG2 and non-cancerous cells like HCT116, FHC, and HeLa, based on varying endogenous levels of the biomarkers. Further investigations have shown that exposure to exogenous hydrogen peroxide (H_2O_2) can induce an increase in endogenous H2S and hNQO1 production, indicating a potential synergistic antioxidant mechanism during oxidative stress. This distinct sensitivity and specificity of the probe are essential for differentiating cancer cell types and provide a valuable tool for classifying cancers based on distinct biomarker profiles.

In a parallel stride, Yuan and colleagues reported an advanced AND-gate bioluminescent probe, **FK-Luc-BH**, engineered for targeted tumor imaging [69]. This probe, capitalizing on the molecular logic gate concept, is tailored to detect the simultaneous presence of two specific tumor biomarkers, cathepsin L and hypochlorous acid (ClO^-), thus enhancing the precision of imaging and reducing the likelihood of false positives. The **FK-Luc-BH** probe employs a dual-locked mechanism where the amino group of NH_2-Luc is conjugated with a cathepsin L-recognizing substrate FK, and its carboxyl group is linked to a ClO^- sensitive benzoylhydrazine moiety (Fig. 4f). As shown in Fig. 5e and **f**, bioluminescence (BL) intensity from 4T1-fLuc tumors in the FK-Luc-BH group (top row) increased significantly after injection, peaking at 20 min and retaining over 59 % of the signal even at 120 min. This indicates that FK-Luc-BH responds rapidly to ClO^- and CTSL, producing NH_2-Luc for BL generation. In contrast, the control group (Ac-Luc-EA) showed much lower BL intensity at 20 min, with signals becoming nearly undetectable by 80 min due to its non-responsive structure. Additional controls (taurine + FK-Luc-BH, E−64d + FK-Luc-BH, and taurine + E−64d + FK-Luc-BH) exhibited reduced expression of ClO− or CTSL, resulting in significantly lower BL signals compared to the FK-Luc-BH group. Quantitative analysis confirmed that the BL intensities for these control groups were 1.76-, 3.29-, and 3.86-fold lower than the FK-Luc-BH group at 20 min. These results demonstrate the effectiveness of FK-Luc-BH for sensitive and efficient imaging of tumor cells co-expressing ClO^- and CTSL (Fig. 5g). These findings illuminate the probe's potential in facilitating precise and specific tumor imaging, heralding a promising avenue for enhancing diagnostic accuracy in oncology.

2.2.4. AND-logic gate probes activated by bioactive small molecules and the tumor microenvironment

In the context of oncological research, the significance of endogenous formaldehyde levels, particularly elevated in cancer cells, cannot be overstated [70]. With concentrations ranging from 100 to 400 μM within cells and about 100 μM in the blood [71], clinical data further reveal that cancerous tissues possess 2 to 8 times higher formaldehyde levels than adjacent normal tissues [70], indicating its potential role in carcinogenesis and tumor progression [72]. Yuan et al. introduced a novel "dual-key-and-lock" probe, **Ru-FA**, a ruthenium complex engineered to detect formaldehyde within cancer cell lysosomes and tumors [73]. **Ru-FA** employs a luminophore-responsive linker-quencher mechanism, combining a Ru-(bipyridine)$^{2+}_{32}$ unit with a 2,4-dinitrobenzene (DNB) group via a formaldehyde-sensitive linker (Fig. 6a). Initially, Ru-FA exhibits low luminescence due to a photoinduced electron transfer from the Ru (II) center to the DNB group. However, when it reacts with formaldehyde in an acidic setting, DNB is detached, activating the Ru(II) complex derivative, **Ru-NR**, and enhancing luminescence. This enhancement in luminescence is attributed to the disengagement of DNB, facilitated by formaldehyde's interaction, which in turn alters the electron transfer dynamics within the Ru-FA complex, thereby activating the Ru(II) complex derivative, Ru-NR. Ru-FA's effectiveness was validated by its capacity to detect lysosomal formaldehyde in cancer cells, marked by a notable increase in luminescence upon interaction with formaldehyde in acidic environments. Quantitative luminescence analysis in various cancer cells corroborated the probe's sensitivity and specificity, indicated by significant Pearson's and Mander's coefficients. This study highlights the role of formaldehyde in tumor biology and showcases Ru-FA's potential in cancer diagnosis and monitoring, offering a new tool for investigating formaldehyde's role in cancer progression and the therapeutic monitoring of its metabolism within tumors.

Exploring further into the dynamics of the tumor microenvironment and its implications for cancer progression, it is imperative to consider the characteristically acidic conditions of cancerous tissues. This acidity, alongside the increased ATP demand from rapidly proliferating cancer cells, plays a crucial role in oncogenic activity [74–76]. Addressing this, Kyo Han Ahn et al. harnessed these environmental factors to develop the ultrafast ATP-Proton AND-Gate probe **5**, aimed at precisely identifying invasive regions in human skin tumors [77]. This probe features a rhodamine 6G core linked to an ATP-binding site on the lactam ring, engineered to enhance fluorescence in response to the acidic conditions within the tumor (Fig. 6b). To overcome the constraints associated with traditional rhodamine-based ATP probes, the research team implemented crucial structural modifications. These include substituting rhodamine B with rhodamine 6G and introducing a cyclohexyl-diamine analogue to increase steric strain around the lactam ring, significantly accelerating the probe's response time from several minutes to nearly instantaneous. This rapid response capability allows the probe to distinguish between tumor cells in active proliferation and those that are quiescent by detecting variations in ATP levels, which reflect the metabolic state of the cells. The probe's effectiveness in utilizing the combined indicators of ATP abundance and acidic tumor conditions provides a deeper insight into cellular metabolism within tumors. According to the study, the probe shows enhanced fluorescence in cancer cells during the S and G2/M phases of the cell cycle compared to the G1/G0 phase. This distinction furnishes a

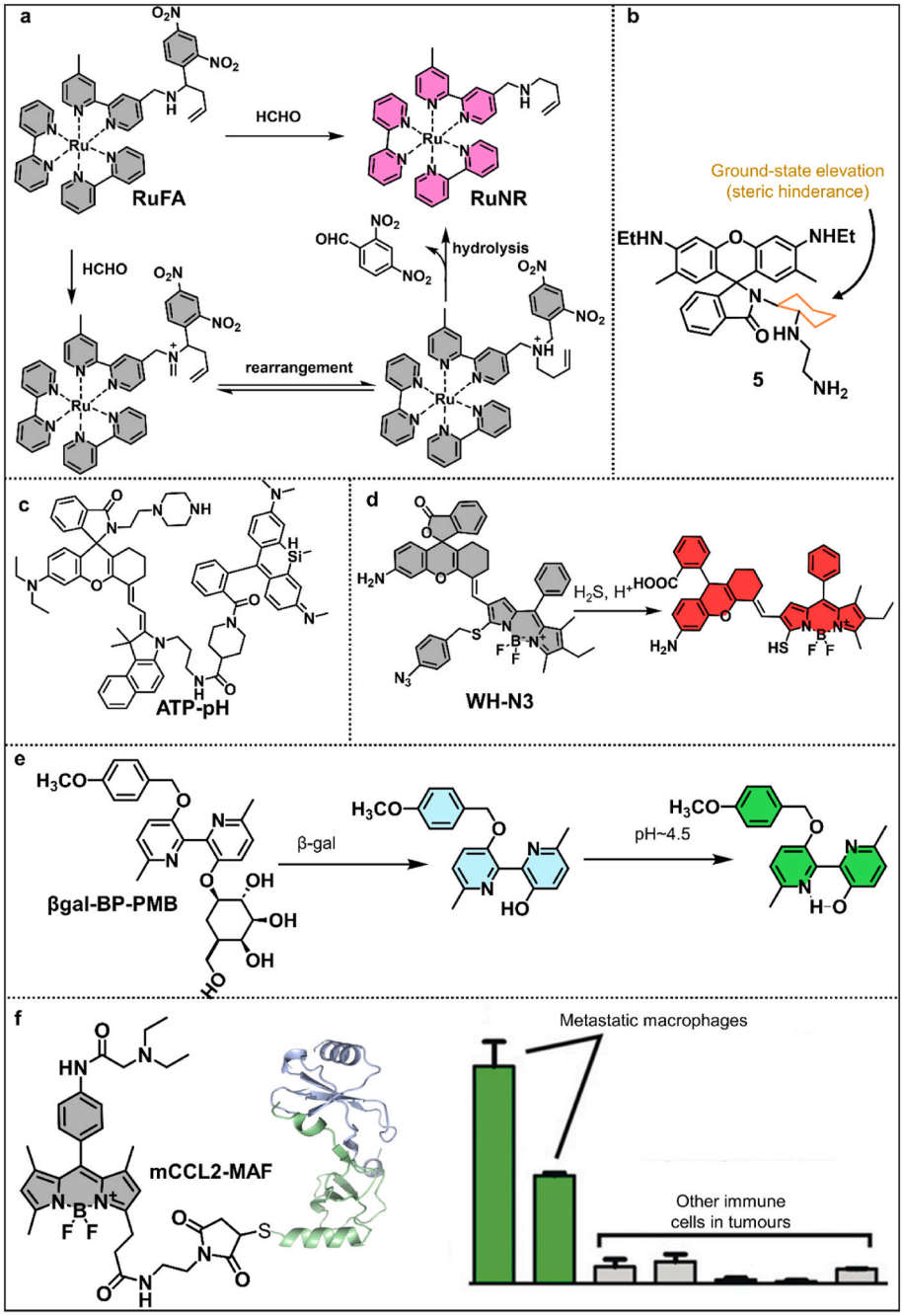

Fig. 6. Representative structures of AND-logic gate fluorescent probes for tumor imaging. (a) Chemical structure of **Ru-FA** and its reaction mechanism with Formaldehyde in an acid microenvironment; (b) The design of Probe **5**, which incorporates high steric strain around the lactam ring, thereby increasing the ground state energy and improving the probe's reactivity to protons and ATP; (c) Structure of probe **ATP-pH**; (d) The response mechanism of the NIR-II fluorescent probe **WH-N3**, which functions on a "dual-lock-dual-key" basis; (e) The structure of probe **βgal-BP-PMB** and its sequential dual-responsive action in the presence of β-galactosidase and at pH 4.5. (f) The molecular design of the probe **mCCL2-MAF** and its preferential effectiveness in targeting metastatic macrophages within tumor environments (Fernandez et al., 2019).

real-time method to differentiate states of cellular proliferation, offering a sophisticated tool for monitoring and understanding tumor biology.

Building upon the concept of dual-responsive probes, Yuan Lin et al. furthered this field by developing the **ATP-pH** probe, a near-infrared reversible probe for both fluorescence and photoacoustic ratiometric imaging of tumors [78]. Constructed with silicon rhodamine as the donor and CS dye as the acceptor, this probe integrates ATP and H^+ recognition units in a specific arrangement that

facilitates dual-stimulus responsiveness (Fig. 6c). A key feature of this probe is the inclusion of a piperidine-4-carboxylic acid linker in the energy-transfer dyad, which increases steric hindrance to stabilize the silicon rhodamine against the high glutathione (GSH) concentrations typical in tumor environments. The probe's design enables gradual activation in response to ATP and H^+ ions, allowing for reversible activation and precise imaging within tumor microenvironments. *In vivo* tests demonstrated its efficacy, with the photoacoustic imaging showing an increasing intensity ratio PA740/PA680, peaking 4 h post-injection. Fluorescence imaging revealed a significantly higher fluorescence intensity ratio in tumor tissue compared to normal tissue post-tumor resection. This specific ratiometric imaging capability of **ATP-pH** underlines the probe's utility in guided tumor resection, significantly advancing tumor imaging techniques.

Further enhancing imaging precision, Liu et al. introduced the **WH-N3** probe, utilizing a "Dual-Lock-Dual-Key" strategy to specifically identify and guide the excision of orthotopic colon cancer [79]. This probe consists of two functional "locks": a rhodamine segment that follows a carboxylic acid-controlled spirocyclization mechanism and an azide group that acts as a highly specific H2S

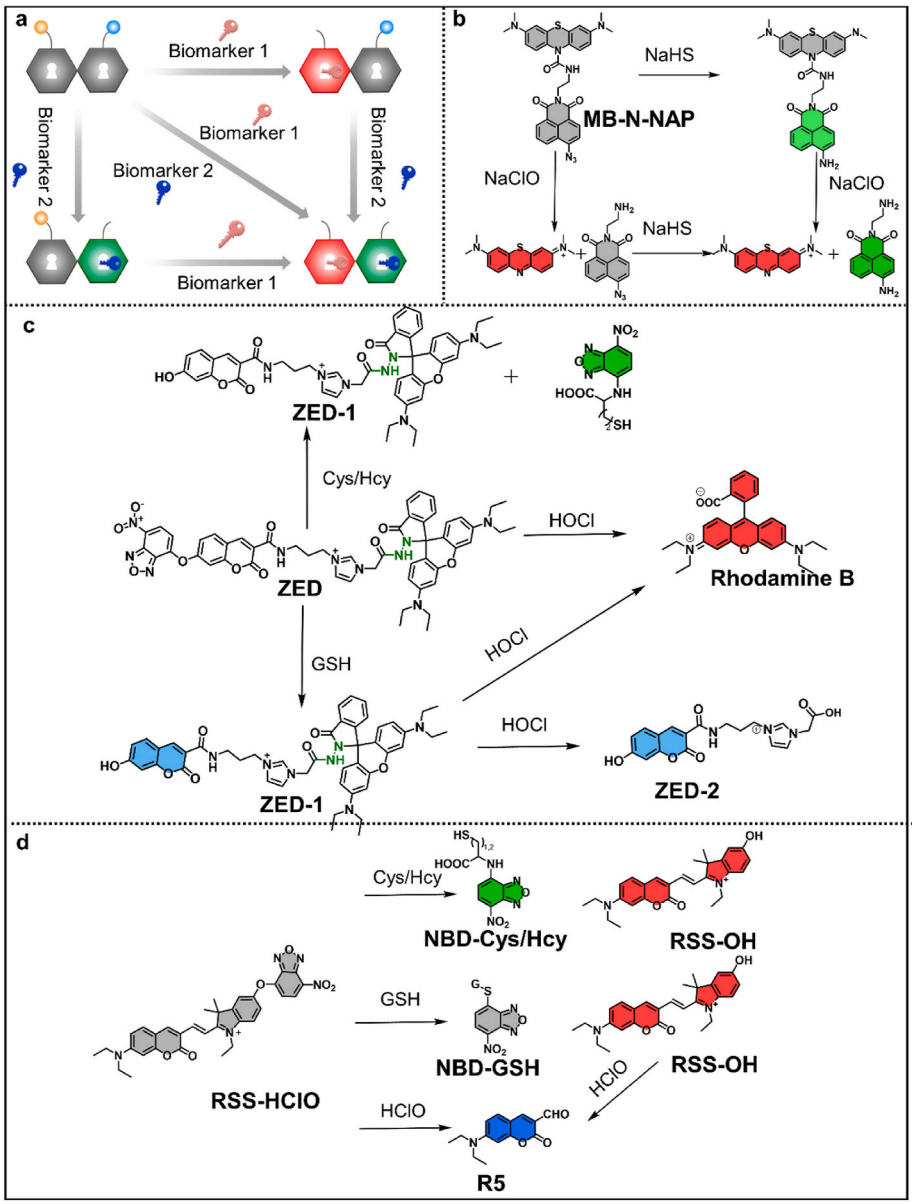

Fig. 7. AND-gates fluorescent probes with two independent optical channels. (a) Schematic representation of an AND-logic gate probe featuring two independent fluorescent signaling groups. Each group responds to a different biomarker, generating distinct fluorescent signals; (b) Structure and activation mechanism of **MB-N-NAP** in the presence of NaHS and NaClO, leading to a change that triggers fluorescence emission; (c) Structure of **ZED** and its stimulus-response performances; (d) Mechanism of action for the **RSS-HClO** probe in differentiating between Cys/Hcy, GSH, and HClO.

recognition site and fluorescence quencher (Fig. 6d). The probe's fluorescence is initially inhibited by an intramolecular charge transfer from the BODIPY fluorophore to the rhodamine derivative. Activation occurs only in the presence of overexpressed H2S and acidic conditions, enhancing its specificity and minimizing nonspecific activation. This activatable probe achieves a high tumor-to-normal tissue ratio, enhancing the precision and specificity of in vivo cancer imaging. Fluorescent imaging with **WH-N3** showed pronounced accumulation at the tumor site with distinct NIR-II fluorescence signals, maintaining intensity up to 24 h post-injection. The surgical application of **WH-N3** facilitated precise tumor delineation during resection, with subsequent pathological evaluation confirming the accuracy of the imaging-guided approach. **WH-N3**'s effectiveness in real-time tumor identification and surgical guidance illustrates its potential for diagnosing and treating deep-seated tumors, thus reinforcing the value of sophisticated imaging probes in oncological surgery.

2.2.5. AND-logic gate probes activated by proteases and the tumor microenvironment

In the quest for enhanced cancer diagnostics, Kouichi Ohe et al. reported a dual-responsive probe, **βgal-BP-PMB**, aimed at detecting ovarian cancer cells [80]. This probe features a β-galactosyl moiety that interacts with β-galactosidase, an enzyme highly overexpressed in ovarian cancer cells. Activation by β-galactosidase triggers the release of the photoluminescent p-methoxybenzyl group from the probe, facilitating light emission. Additionally, the probe's 3,3′-dihydroxy-2,2′-bipyridyl core is sensitive to pH changes, enhancing its utility in monitoring acidity fluctuations in the tumor microenvironment (Fig. 6e). The ability of **βgal-BP-PMB** to emit at two distinct wavelengths depending on the encountered stimuli allows for precise differentiation and quantification of enzyme activity and pH, offering a targeted approach for identifying ovarian cancer cells.

Extending this concept to the tumor microenvironment, Fernandez et al. introduced **mCCL2-MAF** (Fig. 6f), a chemokine-based fluorescent probe, hat targets metastasis-associated macrophages within tumors [81]. This probe combines a Cys-modified CCL2 chemokine with a BODIPY-based macrophage-activatable fluorophore and operates on an AND-gate mechanism. It ensures specificity for CCR2+ metastasis-associated macrophages by binding to functional receptors that internalize the probe upon ligand engagement and subsequently trigger fluorescence in response to macrophage activity. The spectral properties of the original BODIPY fluorophore are maintained, enabling pH-dependent activation that highlights active macrophages undergoing phagosomal acidification. Importantly, the probe retains the chemotactic properties of mCCL2, supporting macrophage migration akin to the natural chemokine. The application of **mCCL2-MAF** in vivo has demonstrated its ability to selectively stain and monitor active macrophages, providing deep insights into their role and distribution within the tumor microenvironment. This probe's innovative design and functional integration underscore its potential to inform therapeutic strategies and enhance our understanding of metastasis-associated macrophages' dynamics and their impact on tumor progression.

2.3. Dual-locked probes with two independent optical channels

Dual-locked probes equipped with two independent optical channels significantly advance the accuracy of tumor diagnosis by enabling real-time, concurrent imaging of multiple tumor biomarkers. While traditional probes typically target a single biomarker and may require co-administration for multi-biomarker detection, this method introduces operational complexities and challenges in signal interpretation. These difficulties arise from differences in intracellular distribution, in vivo pharmacokinetics between probes, and the potential for signal interference. However, dual-locked probes with distinct optical channels overcome these limitations, offering a streamlined approach to simultaneously monitor different or interacting biomarkers, thereby providing clearer and more precise diagnostic insights (Fig. 7a).

2.3.1. Dual optical channel probing: bioactive small molecules activation

Hydrogen sulfide (H_2S) and hypochlorous acid (HClO), crucial reactive species within cellular environments, play vital roles in maintaining cellular homeostasis, with their aberrant levels linked to various diseases, including cancer [82,83]. Understanding their interplay in physiological and pathological states is essential, as highlighted by Ren et al., who developed the dual-responsive fluorescent probe, **MB-N-NAP**, for concurrent detection of H_2S and HClO [84]. This probe leverages the reactivity of 4-azido-1,8-naphthalimide towards H_2S and a methylene blue derivative's sensitivity to HClO, yielding green and red fluorescence respectively (Fig. 7b). Its dual detection mechanism-reduction for H_2S and nucleophilic substitution/oxidation for HClO-enables significant fluorescence enhancement. In cell imaging, MB-N-NAP distinguished endogenous levels of these molecules in both normal and cancer cells, particularly showing enhanced specificity for HepG2 cells, suggesting its utility in precise cancer diagnostics.

Mitochondrial dynamics, particularly alterations in membrane potential ($\Delta\psi m$), are critical indicators of cellular health and potential malignancy [85]. The interplay between mitochondria and reactive oxygen species (ROS), with a particular focus on the role of hypochlorous acid (HOCl) in apoptosis and DNA damage, plays a significant role in the progression of cancer [86–88]. Addressing this, Shi et al. introduced a probe named **ZED**, tailored for in vivo detection of key biomarkers associated with carcinogenesis and cancer treatment [89]. The probe is specifically engineered to identify cysteine/homocysteine, hypochlorous acid, changes in mitochondrial membrane potential, and the activation of the mitochondrial permeability transition pore, offering a comprehensive tool for monitoring these critical cellular events in living cells. The molecular architecture of ZED incorporates three specific fluorophores: NBD (NBD-NHR) for cysteine/homocysteine, coumarin (7-hydroxycoumarin) for generating blue fluorescence, and rhodamine B for detecting hypochlorous acid with red fluorescence (Fig. 7c). These fluorophores are interconnected via an imidazolium salt linker, which not only streamlines the probe's structure but also enhances its aqueous solubility and mitochondrial targeting capability. Upon interaction with cysteine/homocysteine, **ZED** transitions to **ZED-1**, releasing 7-hydroxycoumarin and emitting blue fluorescence at 405 nm. In the presence of hypochlorous acid, the rhodamine component emits red fluorescence at 543 nm. Additionally, **ZED**'s

coumarin unit responds to variations in mitochondrial membrane potential with blue fluorescence, while its NBD moiety signals the opening of the mitochondrial permeability transition pore with green fluorescence at 488 nm (Fig. 9a and **b**). This specific and rapid response mechanism ensures minimal cross-talk and high selectivity in cellular environments. Moreover, **ZED** demonstrates the capability to distinguish between MCF-7 and HBL-100 cell lines, underscoring its potential as a diagnostic and therapeutic tool in cancer research. This precision and functionality highlight **ZED**'s value in elucidating the molecular underpinnings of cancer and informing targeted treatment strategies.

Chemotherapy remains a cornerstone in cancer treatment, yet the real-time visualization of reactive sulfur/oxygen species (RS/OS) during such therapies is inadequately addressed, despite the advent of numerous novel anticancer drugs. There is a pressing need for a sophisticated tool to monitor oxidative stress induced by chemotherapy, essential for understanding its mechanism and evaluating treatment outcomes. Ye et al. introduced a versatile multi-responsive fluorescent probe, **RSS-HClO**, designed to detect cysteine (Cys), homocysteine (Hcy), glutathione (GSH), and hypochlorous acid (HClO) across three distinct emission channels, utilizing coumarin-hemicyanine and **NBD** chloride for fluorescence and recognition, respectively [90]. The **RSS-HClO** probe operates by differentiating between three biothiols and HClO, causing distinct colorimetric shifts in blue, green, and red channels (Fig. 5d). The innovative

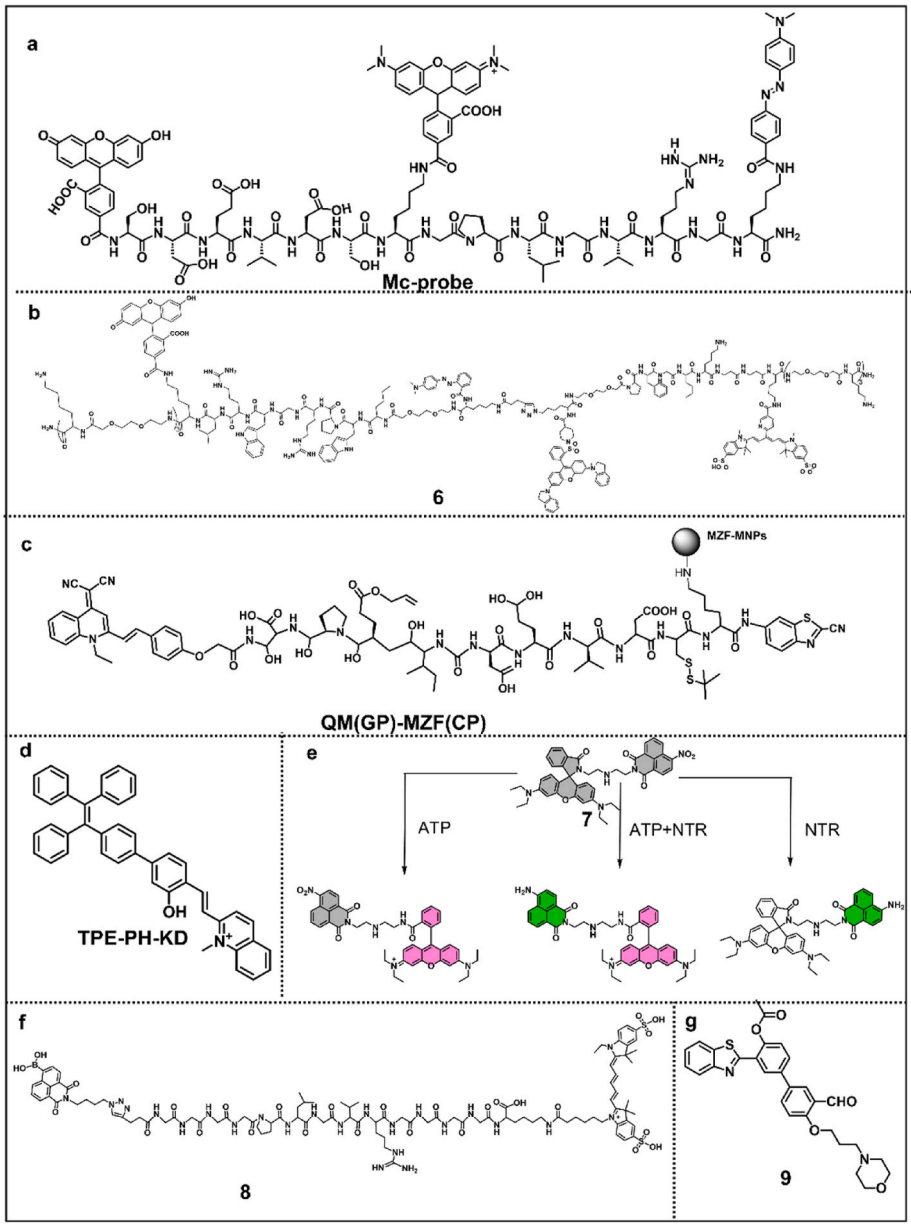

Fig. 8. Chemical Structure of probe **Mc-Probe**, **6**–**9**, **QM(GP)-MZF(CP),** and **TPE-PH-KD**.

application of NBD-Cl and coumarin-hemicyanine as reactive sites facilitates this multiplexed detection. Initially non-fluorescent due to the protected hydroxyl NBD group, RSS-HClO reveals strong red fluorescence upon interacting with biothiols, releasing the RSS-OH moiety. Specifically, the probe exhibits green fluorescence upon binding with Cys/Hcy, while GSH's interaction results in a weaker green fluorescence due to its quenching properties. The introduction of HClO disrupts the C-C bond within the coumarin-hemicyanine structure, eliciting blue fluorescence. This ability to distinguish between biothiols and HClO provides a detailed method for observing RS/OS during chemotherapy, offering direct insights into the oxidative processes crucial for cancer treatment. By facilitating real-time monitoring of these molecules, RSS-HClO enhances our understanding of chemotherapy's cellular impact and assists in refining therapeutic approaches.

2.3.2. Dual optical channel probing: protease activation

In exploring advanced diagnostic strategies, Matrix metalloproteinase-2 (MMP-2) and caspase-3 have emerged as pivotal biomarkers in cancer diagnosis and therapeutic drug screening. Despite the development of numerous selective and sensitive fluorescent probes for MMP-2 and caspase-3, integrating these probes to function synergistically remains challenging due to their distinct localization and metabolic pathways within cells. Addressing this challenge, Zhang et al. reported a novel single-molecular fluorescent probe, **Mc-probe**, designed for the spatiotemporal imaging of MMP-2 and caspase-3 with distinct fluorescence signals [91]. Leveraging a multi-Förster resonance energy transfer (FRET) process, **Mc-probe** responds to MMP-2 and caspase-3 independently through a meticulously engineered molecular structure. The probe consists of an MMP-2 sensitive peptide linker, a caspase-3 responsive peptide, and a combination of FAM/TAMRA/Dabcyl-based multi-FRET donor-acceptor fluorophores (Fig. 8a). This design permits distinct responses to MMP-2 and caspase-3, facilitating high-selectivity and signal-to-noise ratio imaging. Upon interaction with MMP-2, the altered TAMRA/Dabcyl separation distance terminates the FRET process, enabling TAMRA fluorescence recovery. Similarly, caspase-3 activation triggers unique fluorescence emissions due to the probe's specific response to the enzyme, allowing simultaneous imaging of these two biological targets with high specificity and sensitivity.

Moreover, strategies focusing on independent responses have been utilized to detect thrombin and matrix metalloproteinases (MMPs) essential in lung cancer's fibroproliferative activities. Mark Bradley et al. developed a bimodal photonic amplification fluorescent probe **6** designed for the simultaneous detection of thrombin and various matrix metalloproteinases (MMP-2, -9, and -13), which are critical in the fibroproliferative activities associated with lung cancer [92]. The probe employs a FRET-based strategy, incorporating thrombin and MMP peptide-based substrates, along with strategically positioned fluorophores and quenchers (Fig. 8b). This innovative design, synthesized in two segments and assembled using azide/alkyne cycloaddition chemistry, features 5-FAM/-Methyl Red and Cy5/QSY21 fluorophores tagged to thrombin and MMP fragments, respectively. These fragments remain within the hydrophilic tail post-cleavage, enhancing the probe's sensitivity and specificity. The imaging results demonstrated a significant increase in fluorescence signals in lung adenocarcinoma tissue, underscoring the probe's potential utility in guiding biopsies and identifying suspicious lung lesions.

Granzyme B indicates immune system activation, signifying the capacity of cytotoxic T cells to eliminate cancer cells [93,94]. It activates the cascade of cysteine-aspartic acid-specific protease 3 (Caspase-3), a crucial cysteine protease, initiating the apoptosis pathway that targets tumor cells for destruction [94]. Therefore, concurrent tracking of Granzyme B and Caspase-3 offers a comprehensive assessment of the overall success of tumor immunotherapy. Minghua Li et al. introduced **QM(GP)-MZF(CP)**, a dual-modal nanoprobe, to monitor tumor responses in real-time [95]. This probe, employing quinoline-malononitrile (QM) and Mn-Zn ferrite magnetic nanoparticles (MZF-MNPs) as imaging agents, is specifically designed to target granzyme B and Caspase-3 (Fig. 8c). These components are linked with substrate peptides IEPD and DEVD, facilitating the real-time assessment of tumor immunotherapy effectiveness. The probe's unique design allows for the specific cleavage by granzyme B and Caspase-3, enabling detailed monitoring of the activation of cytotoxic T cells and the level of apoptosis in tumor cells.

Two tumor models with differing immunogenic responses were established. The models were divided into four groups: CT26 treated with anti-PD-1 and T cells (anti-PD-1 + T cells (CT26)), 4T1 treated with anti-PD-1 and T cells (anti-PD-1 + T cells (4T1)), a group treated with DOX, and a phosphate-buffered saline (PBS) control group. Treatments were administered every three days for a total of three sessions (Fig. 9c). The real-time monitoring capability of QM(GP)MZF(CP) was then evaluated for assessing the effectiveness of tumor immunotherapy. Results showed that, after the first treatment, the fluorescence signal at the tumor site was significantly higher in the anti-PD-1 + T cells (CT26) group compared to the other three groups (Fig. 9d–h). MRI scans were subsequently performed on mice from each group. As demonstrated in Fig. 4i and j, the T2-weighted imaging (T2WI) enhancement at the tumor sites was modestly higher in the anti-PD-1 + T cells (CT26) and DOX-treated groups than in the other groups, indicating a more pronounced effect in these treatment conditions. The in vivo application demonstrated the probe's effectiveness in providing valuable insights into the dynamic process of tumor response to immunotherapy, highlighting its potential as a significant tool in cancer treatment evaluation.

2.3.3. Dual optical channel probing: tumor microenvironment activation

Vscosity and pH levels within cancer cells are markedly distinct from those in normal cells, marking them as potential biomarkers for cancer detection [96,97]. He et al. introduced a TPE-based fluorescent probe, **TPE-PH-KD** (Fig. 8d), engineered for the dual-channel imaging of pH and viscosity in cellular environments [98]. This probe synergizes a TPE fluorophore with a quinolinium group, where the TPE component serves as a fluorophore and donor, and the quinolinium group acts as an acceptor. Viscosity-induced restriction of the double bond rotation between these groups enhances fluorescence intensity, facilitating viscosity measurements. Concurrently, the probe's ortho-phenol moiety is pH-sensitive, undergoing protonation or deprotonation with pH fluctuations, thereby enabling pH-dependent fluorescence responses. In neutral or basic conditions, **TPE-PH-KD** remains predominantly in a

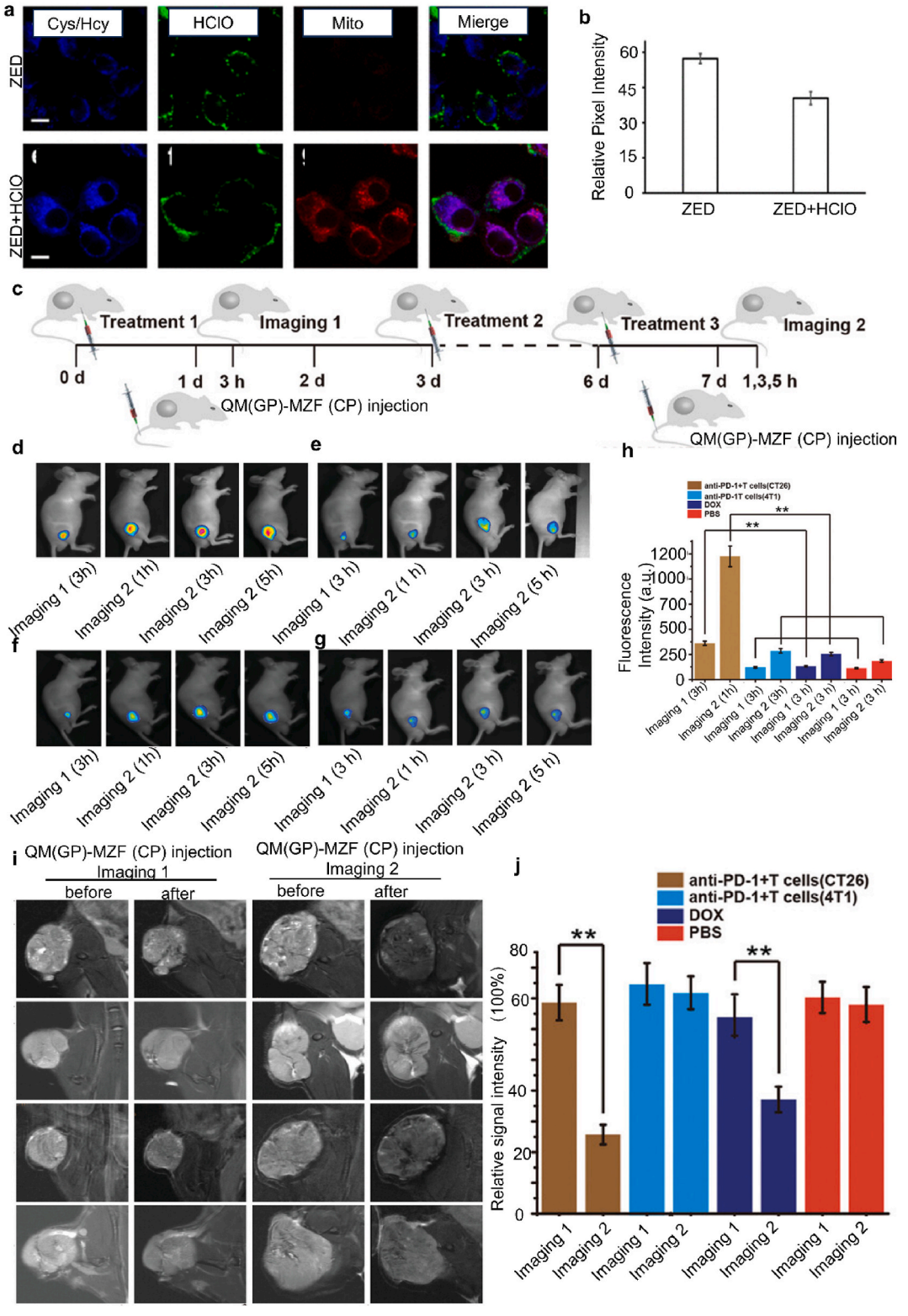

(caption on next page)

Fig. 9. (a) ZED's response to Cys/Hcy, HOCl, and mitochondrial function in A549 cells; (b) Analysis of relative pixel intensity for the images in (a); (c) Schematic diagram showing the immunotherapy regimen and imaging timeline for the animal study. Representative AIE fluorescence images of nude mice with tumors in (d) the anti-PD-1 + T cells (CT26) group, (e) the anti-PD-1 + T cells (4T1) group, (f) the DOX group, and (g) the PBS group at various time points after the first and third treatments (n = 4). (h) Quantitative fluorescence intensity measurements of tumor sites in the different groups after the third treatment; (i) Representative T2-weighted MR images of tumor-bearing nude mice across the different groups before and after injection of QM(GP)-MZF(CP), following the first and third treatments (n = 4); (j) Quantification of T2WI signal intensities at tumor sites in the different groups after the first and third treatments. The above figures are reproduced with permission from references 89 and 95, with authorization for citation.

non-fluorescent deprotonated state, transitioning to a fluorescent protonated form under acidic conditions. This dual responsiveness allows for comprehensive imaging of both pH and viscosity changes within cells. Notably, **TPE-PH-KD** targets lysosomes and mitochondria in cancer cells, offering pH and viscosity-sensitive fluorescence, characterized by a substantial Stokes shift and high selectivity. The probe's efficacy was demonstrated through its ability to monitor intracellular pH and viscosity alterations following treatment with various agents and to differentiate cancer cells from normal ones, with cancer cells exhibiting enhanced fluorescence. Fluorescence intensities across different cancer cell lines followed the order: BT474 > 4T1 > A549 > HepG2 > HeLa. Furthermore, **TPE-PH-KD**'s utility extended to in vivo applications, where it selectively illuminated tumors in tumor-bearing mice, underscoring its potential as a precise tool for tumor visualization at the organ level.

2.3.4. Dual optical channel probing: bioactive molecules and protease activation

The dynamics of intracellular ATP during hypoxic events and its role as a marker responsive to hypoxia are critical yet not fully elucidated. Investigating cellular hypoxia by simultaneously monitoring intracellular nitroreductase (NTR) and ATP levels could provide deeper insights into cancer cell behavior. Ma and colleagues developed a dual-function fluorescent probe **7** monitor hypoxia in living cells by imaging NTR and ATP [99]. This probe uses naphthalimide and rhodamine as fluorochromes for their superior spectroscopic properties and minimal emission overlap (Fig. 8e). The probe includes nitro and diethylenetriamine groups, selectively responsive to NTR and ATP, respectively. The nitro group in 1,8-naphthalimide, upon reduction by NTR in the presence of NADH, is likely to induce a fluorescence off-on response. Additionally, diethylenetriamine's interaction with ATP, supported by π–π stacking between rhodamine and ATP's adenine, aids in the ring-opening and fluorescence activation. Imaging outcomes in live cells reveal the probe's ability to detect shifts in NTR and ATP levels under varying oxygen levels, showing decreased ATP fluorescence in the red channel and increased NTR fluorescence in the green channel as oxygen levels decline. This capacity to monitor NTR and ATP alterations in response to hypoxia may lead to new diagnostic and therapeutic methods that are specifically tailored to the hypoxic conditions prevalent in tumor microenvironments.

The interplay of intracellular and extracellular molecular components, notably reactive oxygen species (ROS) and matrix metalloproteinases (MMPs), plays a pivotal role in the mechanisms underlying cancer invasion and metastasis [100,101]. developed a multicolor fluorescence probe **8** capable of simultaneous imaging of ROS and MMPs within cancer cells, addressing their critical functions in tumorigenesis [102]. This probe, by linking a H_2O_2-responsive fluorophore donor to an MMP2-sensitive peptide with a FRET Cy5 acceptor, enables specific detection of ROS and MMP activities (Fig. 8f). MMP-2's ability to hydrolyze the peptide sequence PLGVR is integral to the probe's function, facilitating distinct fluorescence changes upon MMP2 interaction. The probe's design, featuring a GGGGPLGVRGGGG sequence as the MMP2 substrate, allows for the dual sensing of H_2O_2 and MMP2, illustrating its utility in monitoring cellular signals related to cancer progression. Imaging studies with this probe demonstrated its efficacy in differentiating cell types by MMP2 expression levels, showcasing its potential in evaluating cancer cell metastatic capabilities. Specifically, the probe distinguished between highly invasive MDA-MB-231 cells and less invasive RAW264.7 and MCF7 cells through differential fluorescence signaling, underscoring its application in advanced cancer diagnostics and treatment planning.

Cellular oncogenic transformation, lipase activity remains consistent, in contrast to hydrogen sulfide (H_2S) levels, which notably escalate in certain cancer phenotypes. This differential expression of lipase and H_2S between normal and malignant cells provides a basis for their discrimination. Liu et al. crafted a lysosome-targeted, dual-site fluorescent probe **9**, discerning cancer cells from normal counterparts by exploiting variations in H_2S concentration [103]. This probe integrates a benzothiazole unit, cleavable by porcine pancreatic lipase (PPL), and a morpholine component for lysosomal localization, alongside a thiol group reactive towards H_2S, facilitating its detection (Fig. 8g). In the presence of PPL, the probe emits yellow fluorescence, transitioning to blue with concurrent PPL and H_2S exposure, indicative of cancerous cells. Such chromatic shifts enable the probe to distinguish between cancerous and non-cancerous cells through H_2S quantification, presenting an innovative avenue for cancer diagnostics and cellular differentiation.

3. Dual-locked probes for tumor treatment

Dual-locked probes are at the forefront of oncological innovation, offering a refined method to boost the specificity and potency of cancer treatments. These probes are crafted to activate only in the presence of two specific tumor-associated signals, substantially lowering the likelihood of off-target effects and heightening the accuracy of the therapy. In tumor treatment scenarios, these probes are adaptable to various stimuli combinations, such as particular enzymes, pH fluctuations, or distinct biomolecules predominantly found or amplified in tumor cells. When these predefined conditions are concurrently satisfied, the probes initiate a structural alteration, prompting the release of a therapeutic agent or the generation of a tumor-specific diagnostic signal. This dual-trigger activation mechanism ensures the direct targeting of cancer cells, thereby minimizing harm to normal tissues and enhancing patient prognoses. This strategy embodies the ethos of personalized medicine, advocating for therapies that are meticulously tailored to the individual

characteristics of each patient's disease.

3.1. Sequentially activated prodrug

Traditional chemotherapy is known for its adverse side effects, attributed to its indiscriminate action on both healthy and tumor tissues. Targeted prodrugs, activated by endogenous substances within the tumor microenvironment, offer a solution by releasing active drugs specifically at tumor sites, thereby mitigating toxic side effects [104]. Despite the widespread application of targeted prodrugs in cancer treatment, a significant issue they face is the side effects caused by the "off-target effect [105]. The intricate biological microenvironment complicates the precise activation of even well-engineered prodrugs. Enhancing treatment specificity through the design of drugs and probes responsive to multiple cancer-specific biomarkers ensures that prodrugs are activated solely in the presence of a confluence of these biomarkers, reducing undesired side effects [106–109] (Fig. 10a). Huang and colleagues introduced an innovative dual biomarker cascade-activated prodrug strategy for melanoma treatment, aimed at overcoming the limitations of traditional chemotherapy [110]. The prodrug, Coumarin-Quinazolinone-phenylBoronic acid pinacol ester (**CQB**), is engineered for selective activation by melanoma-overexpressed reactive oxygen species (ROS) and tyrosinase. **CQB** comprises Coumarin-Quinazolinone (CQ) for mitochondrial targeting and monitoring, and phenylboronic acid pinacol ester as a cascade-activated pro-warhead (Fig. 10b). Upon encountering ROS and tyrosinase within melanoma cells, CQB is transformed into its active form, Coumarin-Quinazolinone-o-Quinone (CQQ), featuring an o-quinone group as the reactive entity. Fig. 11a shows that CQB selectively induced ROS accumulation in B16 cells, with no change in ROS levels in LO2, HepG2, and HEMs cells. This disruption of redox homeostasis in B16 cells was further confirmed by a significant reduction in the GSH/GSSG ratio upon **CQB** treatment, while no changes were observed in the other cell lines (Fig. 11b). CQB treatment resulted in a significant reduction in mitochondrial membrane potential (MMP) in B16 cells, suggesting that CQB induces mitochondria-mediated apoptosis (Fig. 11c–e). Additionally, in vivo tests on a B16 xenograft mouse model affirm the strategy's potential for targeted melanoma treatment. This research illuminates a promising avenue for developing targeted melanoma therapies and possibly for other cancer types, exploiting specific cancer cell biomarkers to attain selective and efficacious treatment.

Based on similar design strategies, Liu et al. developed a dual-activated prodrug, **BTC** (Fig. 10c), for the integrated chemo-photodynamic treatment of breast cancer [111]. This innovative prodrug combines a glutathione (GSH)-sensitive BODIPY-based

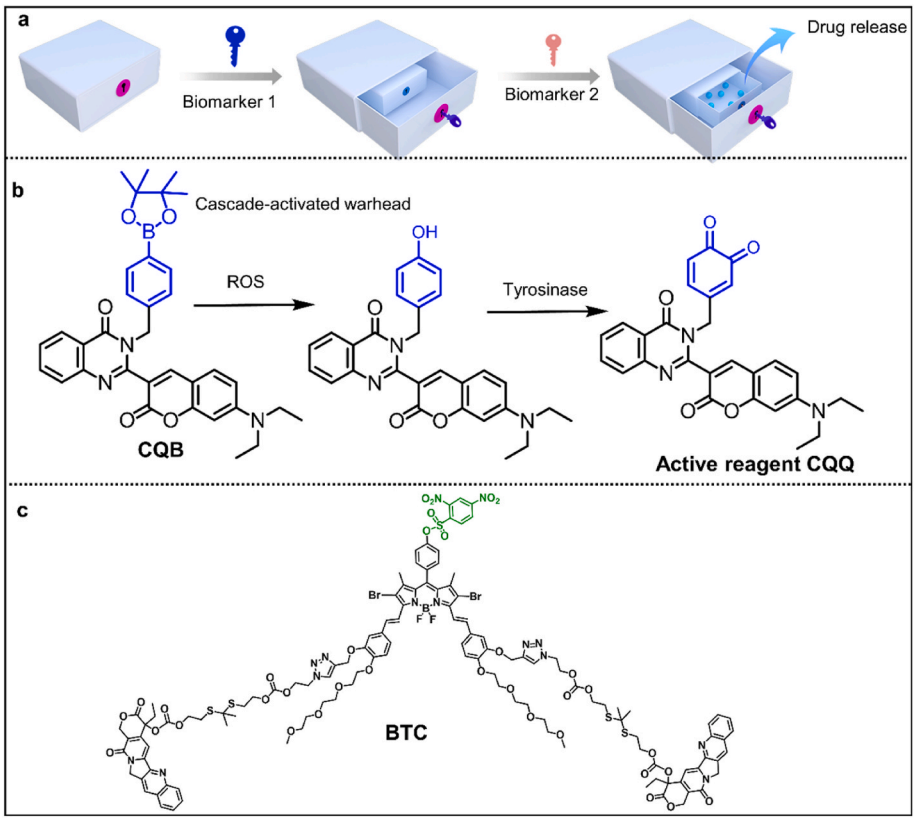

Fig. 10. Sequentially activated prodrug. (a) Schematic illustration showing a dual-locked prodrug activated by two different biomarkers. The presence of each biomarker in the tumor environment triggers a sequence that culminates in the targeted release of therapeutic agents; (b) Chemical transformation of the cascade-activated warhead CQB in the presence of reactive oxygen species (ROS) and the enzyme tyrosinase, leading to the formation of the active reagent CQQ; (c) Molecular structure of the BTC probe.

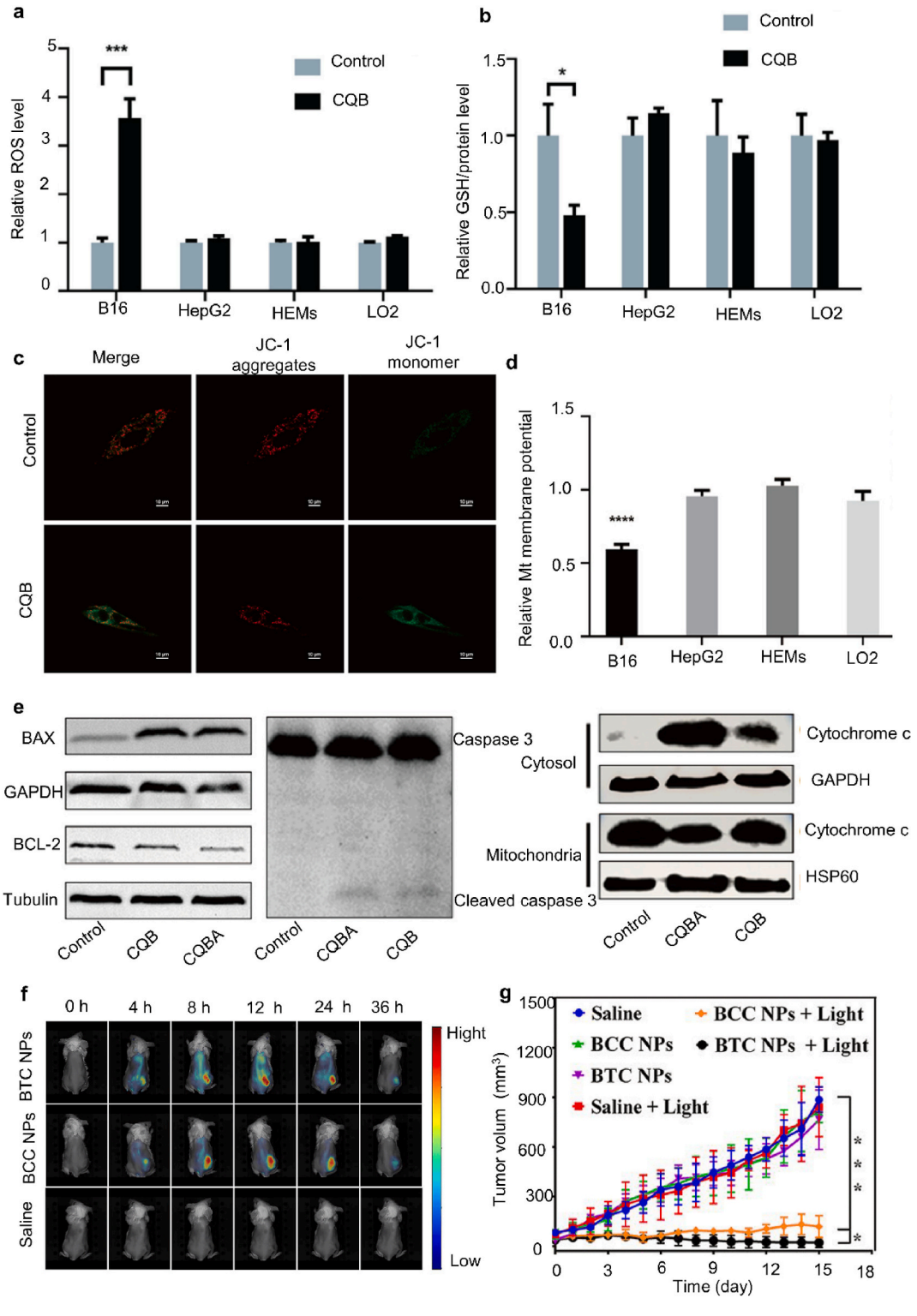

(caption on next page)

Fig. 11. (a and b) Comparative analysis of reactive oxygen species (ROS) levels and GSH/Protein ratios in B16 melanoma cells, HepG2 liver cancer cells, normal human epidermal melanocytes (HEMs), and LO2 hepatocytes after exposure to 20 μM **CQB**. Statistical significance: *p < 0.05, ***p < 0.001; (c) Assessment of mitochondrial membrane potential (MMP) in B16 cells post-treatment with **CQB**, visualized using JC-1 fluorescent dye; (d) Quantitative measurement of MMP across various cell lines treated with **CQB**; (e) Western blot analysis of apoptosis markers in B16 cells following exposure to 20 μM CQB, CQBA, or control treatment; (f) In vivo fluorescence imaging of 4T1 tumor-bearing mice at different intervals post-administration of **BTC** nanoparticles (NPs), BCC NPs, or saline solution; (g) Tumor progression in BALB/c mice monitored through growth curves under the different treatment regimens. The above figures are reproduced with permission from references 110 and 111, with authorization for citation.

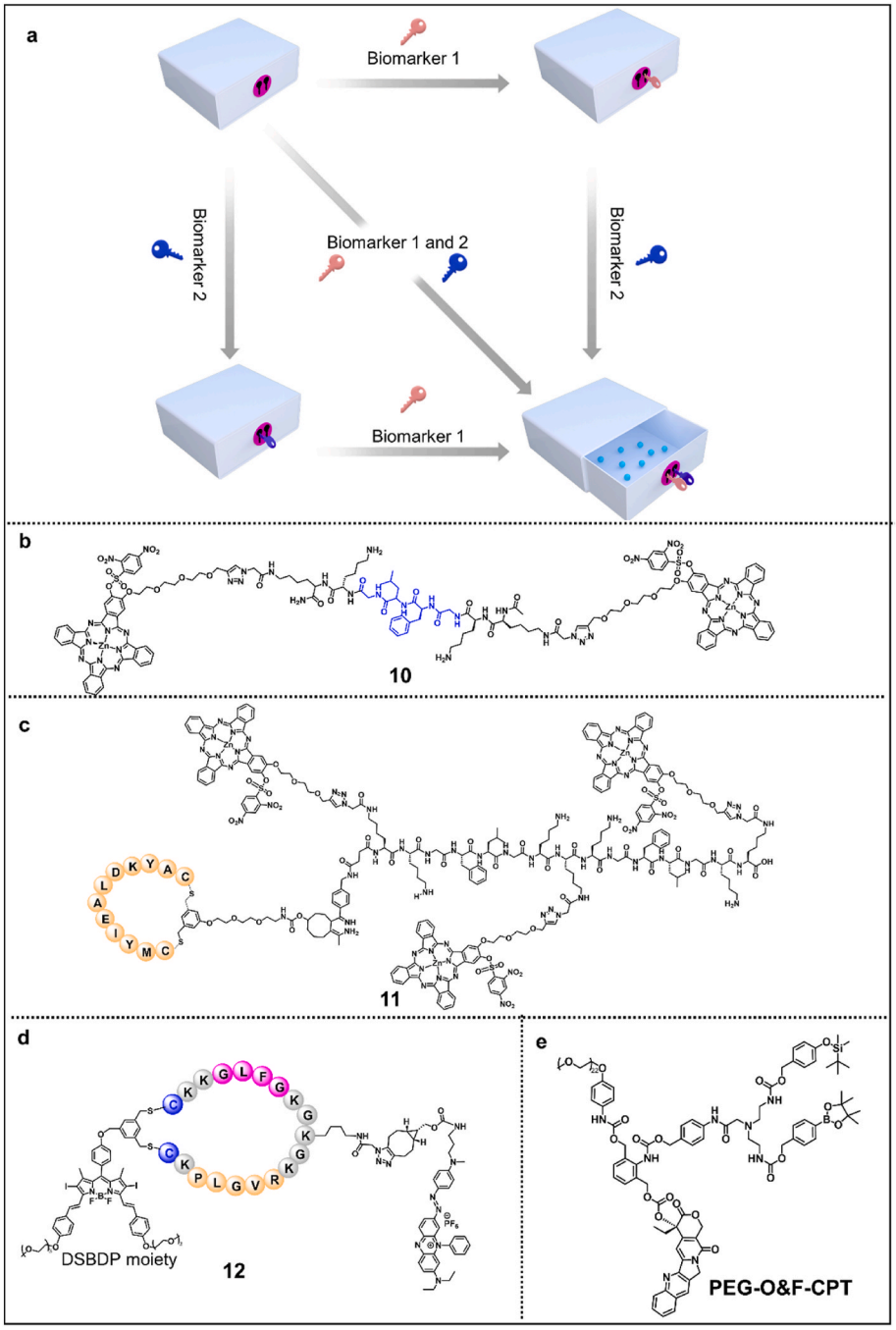

Fig. 12. AND-logic gated prodrug. (a) Schematic representation of a dual-lock prodrug system that activates drug release only when both biomarkers are simultaneously present, ensuring targeted therapeutic action; (b–e) Chemical structure of probe **10**–**12** and **PEG-O&F-CPT**.

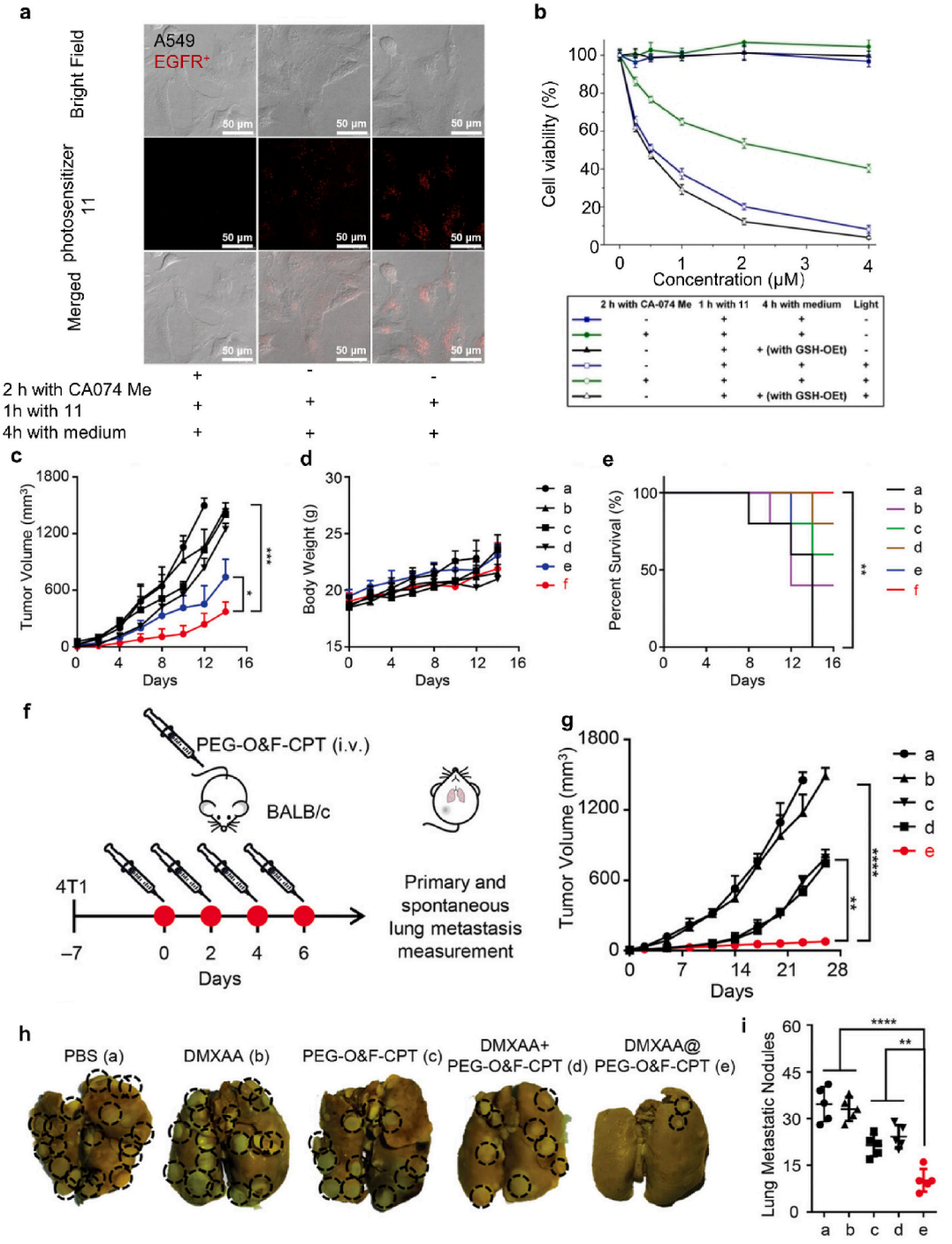

Fig. 13. (a) Bright field, fluorescence, and merged images of A549 cells after incubation with or without CA-074 Me (25 μM) for 2 h, followed by treatment with photosensitizer 11 for 1 h, and an optional 4-h post-incubation. (b) Cytotoxic effects of photosensitizer 11 on A549 cells under dark and illuminated conditions ($\lambda > 610$ nm, 23 mW/cm^2, 28 J/cm^2); (c) Tumor growth curves for different treatment groups; (d) Body weight curves of mice after treatments; (e) Survival curves of mice across treatment groups; (f) Schematic of intravenous treatments for 4T1 breast tumor and lung metastasis in BALB/c mice with primary tumors (50 mm^3). Treatments included PBS, free DMXAA, PEG-O&F-CPT micelles, a mixture of DMXAA with PEG-O&F-CPT micelles, or DMXAA@PEG-O&F-CPT micelles every other day for four doses (10 mg/kg CPT, 8 mg/kg DMXAA). For groups (c–e), BAA (30 mg/kg) was injected at 24 and 36 h post-treatment; (g) Average tumor growth curves (n = 6); (h) Lung tissue images on day 26, with metastatic lesions marked; (i) Number of lung metastatic nodules on day 26 (n = 5); The above figures are reproduced with permission from references 113 and 115, with authorization for citation.

photosensitizer, exhibiting photoinduced electron transfer (PET) effects, with a thioketal linker responsive to reactive oxygen species (ROS), attaching it to the chemotherapeutic agent camptothecin (CPT). Within tumor cells, the prodrug is activated by elevated GSH levels, initiating the BODIPY photosensitizer and producing ROS upon light activation. Subsequently, the ROS-mediated cleavage of the thioketal linker releases CPT, enabling simultaneous photodynamic and chemotherapy. In vitro assays with breast cancer cell lines 4T1 and MCF-7 demonstrated that BTC effectively induces cell death by activating the BODIPY photosensitizer, generating ROS, and releasing CPT upon light exposure. In vivo, using 4T1 tumor-bearing mice, BTC showcased passive tumor targeting through the enhanced permeability and retention (EPR) effect, resulting in effective combined treatment (Fiure11f and 11g).

These results highlight BTC's potential as a dual-activated nano-prodrug, offering a promising, efficacious approach for breast cancer therapy, validated in both cell culture and animal models.

3.2. AND-logic gated prodrug

The "AND" logic-gated prodrug, requiring simultaneous presence of dual biomarkers for activation, offers significant potential for enhanced tumor specificity (Fig. 12a). Pui-Chi Lo et al. have innovated smart photosensitizer **10** for targeted photodynamic therapy in cancer cells [112]. Photosensitizer **10** is tailored to respond specifically to the cancer cell microenvironment, reacting to elevated glutathione (GSH) and cathepsin B levels, hallmarks of cancer cells. Photosensitizer **10** incorporate GSH-responsive 2,4-dinitrobenzenesulfonate (DNBS)-substituted zinc(II) phthalocyanine (ZnPc) units linked via cathepsin B-cleavable peptide linkers, maintaining a quenched state until they engage with both GSH and cathepsin B (Fig. 12b). Activation triggers a release of phthalocyanine units, enhancing cytotoxic effects under light exposure. The photosensitizer **10** also demonstrate dynamic intracellular fluorescence changes in response to GSH ester and cathepsin B inhibitor treatments, highlighting their potential for precision in targeted photodynamic therapy. In light-exposed conditions, the photosensitizer **10** exhibit significant cytotoxicity, with IC50 values between 0.21 and 0.39 μM, dependent on intracellular GSH and cathepsin B levels. This suggests their utility as intelligent photosensitizers for targeted therapy. However, while photosensitizer **10** show promise in vitro for targeted photodynamic therapy, further in vivo studies are necessary to fully ascertain their efficacy and safety in clinical settings.

To enhance tumor specificity in photodynamic therapy, Pui-Chi Lo et al. engineered an innovative multifunctional photosensitizer **11** designed for targeted cancer treatment [113]. Photosensitizer **11** features a unique trimeric phthalocyanine core, where each zinc (II) phthalocyanine unit is conjugated with a glutathione (GSH)-responsive quencher and connected through cathepsin B-cleavable linkers (Fig. 12c). This sophisticated design ensures that the PMB remains in a quenched state until it encounters GSH and cathepsin B within the cancer cell microenvironment, allowing for selective activation (Fig. 13a). Further enhancing its targeting capabilities, photosensitizer **11** is equipped with an EGFR-targeting cyclic peptide, augmenting its specificity towards cancer cells expressing EGFR. The efficacy of **11** has been validated across various cancer cell lines, demonstrating a notable 48-fold increase in intracellular fluorescence in response to the dual stimuli, indicative of its cell-selective activation mechanism. Impressively, the photosensitizer **11** shows substantial photocytotoxicity against EGFR-positive cancer cells (Fig. 13b), with IC50 values reaching as low as 0.42 μM and predominantly inducing apoptosis. These results underscore the photosensitizer **11**'s potential as a precise, molecular-based photosensitizing agent for photodynamic therapy, highlighting its dual-stimuli-responsive design and tumor-targeting efficiency. Such advancements signify a significant step forward in developing more targeted and effective photodynamic therapies for cancer treatment.

Subsequently, Pui-Chi Lo et al. elucidated a novel double-locked photosensitizer **12** responsive to two enzymes, designed for targeted photodynamic anticancer therapy [114]. The photosensitizer **12** comprises a distyryl boron dipyrromethene (**DSBDP**)-based photosensitizer linked with a Black Hole Quencher 3 (BHQ-3) moiety through two peptide segments originating from a cyclic peptide, with sequences PLGVR and GFLG (Fig. 12d). These segments act as substrates for MMP-2 and cathepsin B, enzymes predominantly overexpressed in various cancer cells. The photosensitizer **12** remains quenched in its unreacted state and is activated only upon concurrent interaction with MMP-2 and cathepsin B, leading to specific cleavage of the peptide segments and restoration of the **DSBDP** moiety's photodynamic activity. This innovative design grants **12** the functionality of a biological AND logic gate, requiring the presence of both tumor-associated enzymes for activation, thereby heightening its specificity for targeted photodynamic therapy. In vivo experiments involving A549 tumor-bearing nude mice demonstrated that intratumoral **12** administration followed by laser exposure significantly reduced tumor size compared to control groups, showcasing the 12's therapeutic efficacy. Notably, the **12** exhibited pronounced photocytotoxicity against MMP-2-positive cell lines, A549 and U-87 MG, with IC50 values of 0.78 and 0.91 μM, respectively. Crucially, the PMB displayed minimal skin photosensitivity, a significant advantage over the 'always-on' **DSBDP**, which induced considerable skin damage upon light exposure. This property underscores the **12**'s refined photodynamic control, minimizing potential side effects such as skin photosensitivity associated with conventional photosensitizers in photodynamic therapy. These attributes underscore the **12**'s potential as a safe and effective photodynamic therapy agent, offering a strategic approach to cancer treatment with minimized collateral damage.

Expanding upon targeted therapeutic strategies, Chen et al. devised an "AND" logic-gated prodrug micelle system, specifically engineered for the targeted release of therapeutics [115]. This system requires the simultaneous presence of two tumor-specific stimuli-boramino acids (BAA) and reactive oxygen species (ROS)-to activate drug release. The micelles are constructed from a self-assembling amphiphilic polymer-prodrug conjugate, **PEG-O&F-CPT**. This conjugate cleverly combines a hydrophilic polyethylene glycol (PEG) segment with a hydrophobic camptothecin (CPT) drug segment (Fig. 12e). The segments are interconnected via an "AND" logic-gated trigger designed to respond concurrently to the presence of both BAA and ROS, thus ensuring precise drug delivery to targeted cancer cells. Such a design ensures the micelles' disassembly and subsequent CPT release are confined to the tumor microenvironment, thereby enhancing targeting precision and reducing collateral effects on healthy tissue. In contrast to therapies utilizing

a single stimulus, the dual-stimulus treatment demonstrated a rapid and pronounced suppression of tumor growth and extended survival, as anticipated (Fig. 13c and **e**). Moreover, all treatment groups maintained stable body weights (Fig. 13d), indicating a favorable safety profile for the drug. Upon simultaneous recognition of BAA and ROS, the micelles disassemble in a regulated manner, facilitating the targeted release of CPT. Moreover, these prodrug micelles are formulated to deliver STING agonists, thereby eliciting a robust immune response within the tumor milieu. This multifaceted therapeutic modality not only directly curtails tumor proliferation but also modulates the tumor microenvironment to foster an immunological response against cancer cells. In vivo evaluations in murine models of melanoma and breast cancer demonstrated significant tumor suppression (Fig. 13f and **g**) and effective inhibition of lung metastasis (Fig. 13h and **i**), highlighting the superior performance of the micelle system compared to conventional therapies. This research illustrates the synergistic potential of merging synthetic chemistry, nanotechnology, and immunotherapy to forge sophisticated platforms for cancer treatment, emphasizing the system's promise for advancing precision oncology.

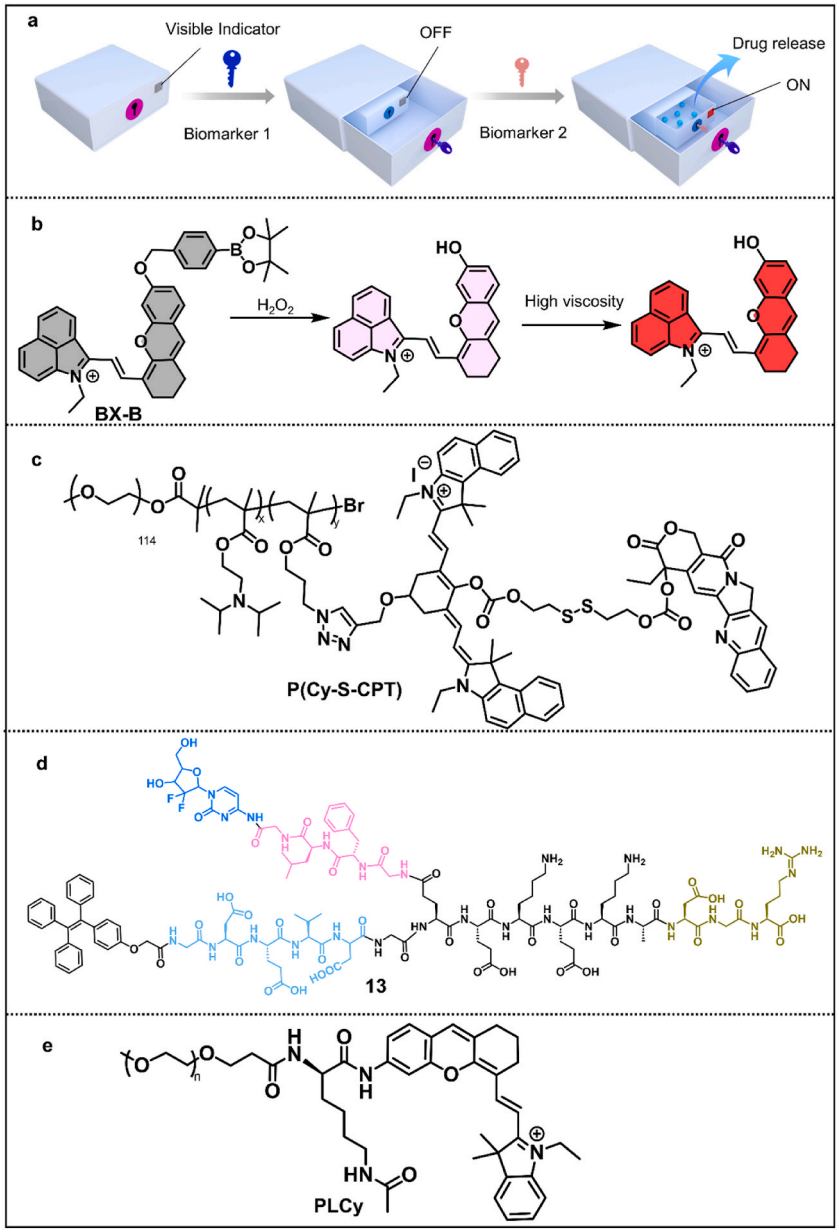

Fig. 14. Stepwise activated dual-lock probes for tumor theranostics. (a) Sequence-activated probe for real-time tracking and programmable drug release; (b) H_2O_2 and viscosity sequentially activated fluorescence probe **BX-B** for cancer phototherapy; (c–e) Chemical structure of probe **P (Cy-s-CPT), 13 and PLCy**.

4. Dual-locked probes for tumor theranostics

In the evolving field of tumor theranostics, dual-locked probes stand at the forefront, offering an integrated diagnostic and therapeutic modality within a singular framework. These probes are meticulously engineered to concurrently detect two specific biomarkers, substantially augmenting their precision and effectiveness in targeting neoplastic cells. The incorporation of an "AND" logic gate ensures that therapeutic interventions are activated exclusively within the tumor milieu, significantly reducing non-specific interactions and enhancing patient prognoses. This section aims to explore the sophisticated architecture, operational principles, and therapeutic implications of dual-locked probes in tumor theranostics, underscoring their contribution to the personalization of cancer management.

4.1. Sequentially activated dual-locked probes for tumor theranostics

The dual-responsive and sequentially activated, coupled with precision targeting, to significantly bolster the effectiveness and accuracy of cancer treatments. By harnessing the potential of critical biomarkers such as hydrogen peroxide, viscosity, pH levels, and enzymes that are disproportionately expressed in cancer cells, these approaches facilitate precise drug delivery. They not only enhance therapeutic efficacy but also offer real-time, actionable insights into the treatment's impact, marking a pivotal step forward in the realm of tumor theranostics (Fig. 14a).

The integration of near-infrared (NIR) fluorescence imaging with the combined strengths of photodynamic therapy (PDT) and photothermal therapy (PTT) presents a promising therapeutic avenue in oncology. Consequently, there is a compelling demand for the development of a dual-key activated fluorescence probe that can simultaneously respond to H_2O_2 and viscosity, thereby augmenting the efficacy of cancer phototherapies. In response to this need, Li and colleagues synthesized a novel NIR-I/II fluorescence probe, designated **BX-B**, specifically engineered for monitoring the effectiveness of combined photodynamic and photothermal therapies in oncological applications [116]. The **BX-B** probe comprises a BODIPY fluorophore for NIR-I/II fluorescence emission, a borate ester group, and a hydroxyl group, which collectively confer sensitivity to H_2O_2 and viscosity (Fig. 14b). The biodistribution and activation of **BX-B** in tumor-bearing mice were assessed after intravenous injection, with fluorescence signals in the NIR-I and NIR-II channels peaking at 8 h post-injection, indicating optimal tumor accumulation and activation for phototherapy (Fig. 15a). Temperature monitoring (Fig. 15b and **c**) demonstrated a marked increase from 35.6 °C to 56.7 °C in the **BX-B** group under laser irradiation, compared to a modest rise in the PBS group. Tumor volume assessments over 14 days (Fig. 15d) confirmed significant tumor reduction only in the **BX-B** group with laser treatment, highlighting its effectiveness in photothermal therapy. Thus, the development of BX-B, which utilizes dual-key activation for NIR-I/II fluorescence imaging-guided synergistic photodynamic (PDT) and photothermal therapy (PTT), offers a promising approach for future cancer treatment, enabling both effective therapy and real-time monitoring of therapeutic outcomes.

Building on this approach, Zhu and colleagues have developed a sophisticated nanoprobe, **P(Cy-S-CPT)**, that utilizes the tumor microenvironment's specific stages for sequential activation [117]. This dual-channel fluorescent nanoprobe, designed with a sequence-activated AND logic gate, enables precise monitoring of drug release in real time within living cells. This nanoprobe is composed of a diblock copolymer with a segment sensitive to pH changes and a dual-channel near-infrared (NIR) fluorescence module, where a Cy5.5 dye is tethered to camptothecin (CPT) via a disulfide bond (Fig. 14c). This intricate design allows P(Cy-S-CPT) to exhibit highly sensitive responses to minor pH fluctuations and elevated biothiol levels in the tumor microenvironment, enabling precise, sequence-activated drug delivery. Initially, the nanoprobe responds to subtle pH variations, disassembling within endosomes/lysosomes, marked by an 830 nm fluorescent signal. Following disassembly, the nanoprobe encounters cytosolic glutathione (GSH) overexpression, triggering a secondary fluorescence at 650 nm, signaling GSH-mediated cleavage post-disassembly. *In vivo* studies with A549 xenograft tumor-bearing mice have showcased the nanoprobe's ability to accumulate specifically in tumor sites, providing real-time dual-channel NIR fluorescence imaging of its disassembly and drug release (Fig. 15e and **f**). **P(Cy-S-CPT)**'s application resulted in a marked tumor volume reduction and a significant inhibition of tumor growth by 93.7 % (Fig. 15g–i). These outcomes affirm **P(Cy-S-CPT)**'s potential as an effective, targeted therapeutic tool for cancer, illustrating its capability for precise, programmable drug release and minimizing off-target effects.

Expanding the scope of targeted treatments, Ji et al. have introduced a novel approach for pancreatic cancer treatment, devising a gemcitabine-based prodrug **13** that is activated through a cascade enzymatic reaction, paired with an aggregation-induced emission (AIE) light-up probe for real-time, in situ monitoring of therapeutic efficacy in pancreatic cancer cells [118]. This prodrug is ingeniously structured, integrating gemcitabine (GEM), a Gly-Phe-Leu-Gly (GFLG) peptide linker, and a specialized Asp-Glu-Val-Asp-Arg-Gly-Asp-Arg-Gly-Asp-Arg-Gly (TPE-DEVD-RGD) probe (Fig. 14d). The GFLG peptide serves as a substrate for cathepsin B, an enzyme abundantly expressed in pancreatic cancer cells, facilitating the release of active gemcitabine and the apoptotic TPE-DEVD-RGD probe upon cleavage. The RGD sequence within the probe targets integrin αvβ3, a receptor overexpressed in these cancer cells, ensuring selective drug uptake and efficacy. Following activation, gemcitabine induces apoptosis, while the TPE moiety, an AIE component, lights up in response to caspase-3 activation, offering a fluorescent marker to track cell apoptosis in situ. This integrated system combines targeted drug delivery and apoptosis induction with a novel imaging capability, enabling noninvasive monitoring of the treatment's effectiveness directly within pancreatic cancer cells. This approach represents a significant step forward in personalized cancer therapy, offering a multifunctional platform for precise drug delivery and real-time monitoring of therapeutic outcomes in pancreatic cancer treatment.

Furthermore, Yuan et al. have developed **PLCy**, an advanced macrotheranostic probe designed for mitochondria-specific tumor imaging and therapeutic applications [119]. The probe consists of a near-infrared (NIR) fluorophore, hemicyanine (CyNH2), which is

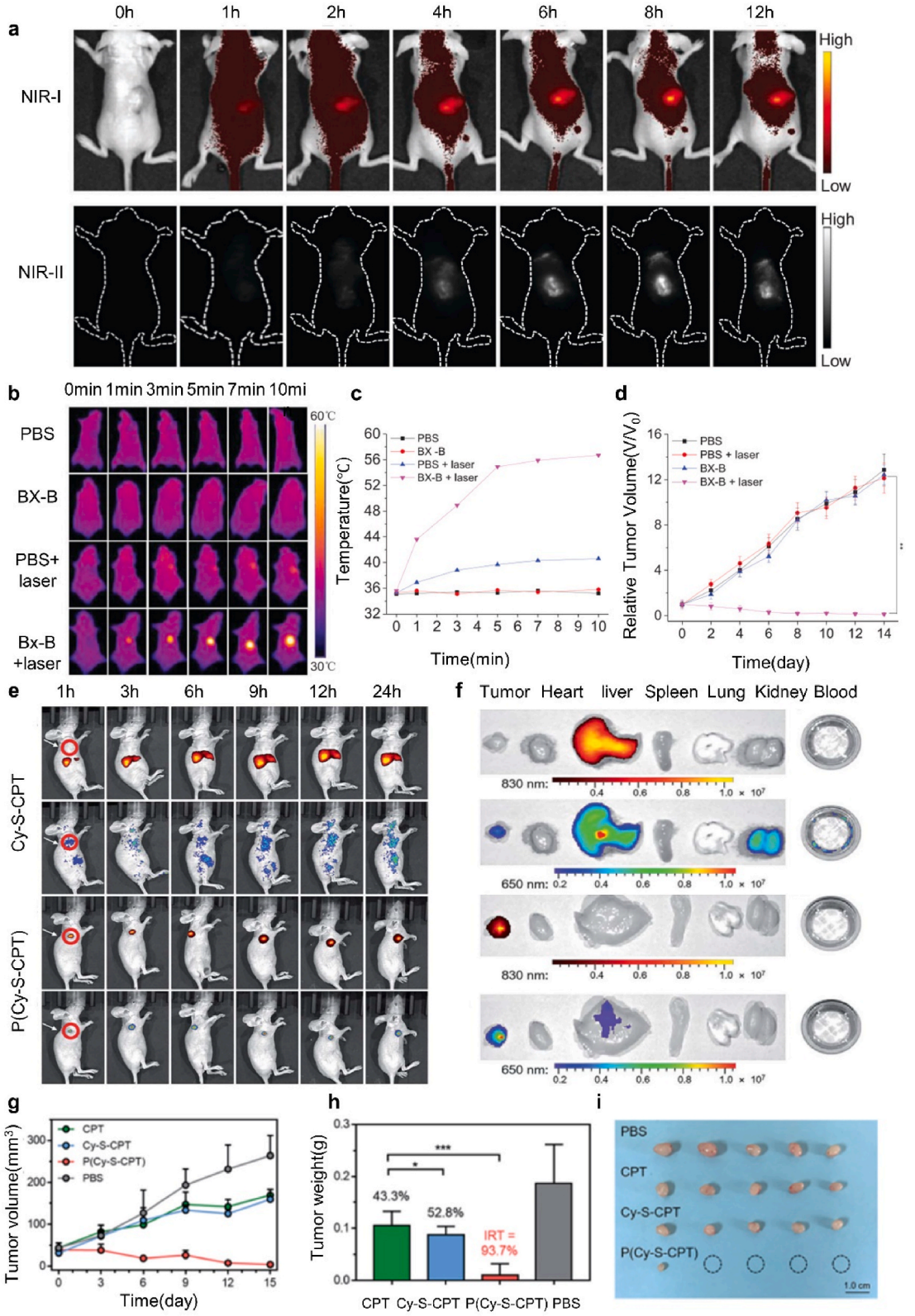

(caption on next page)

Fig. 15. (a, b) NIR-I and NIR-II fluorescence imaging of tumor-bearing mice post-injection of BX-B (500 μM) at various time points (0, 1, 2, 4, 6, 8, 12 h); (c, d) Photothermal imaging and corresponding temperature changes of tumor sites after different treatments; (e) Tumor volume changes over time for various treatments (n = 3, mean ± SD, **p < 0.01, ***p < 0.001); (f) Dual-channel NIR fluorescence imaging of A549 xenograft-bearing mice at different intervals (1, 3, 6, 9, 12, 24 h) following intravenous injection of Cy-S-CPT and P(Cy-S-CPT) at a dose of 0.1 mg/kg CPT-equivalent; (g) Ex vivo NIR fluorescence of major organs and tumor tissue, 24 h post-injection; (h) Antitumor efficacy of the sequence-activated nanoprodrug in A549 xenografts, comparing PBS, CPT, Cy-S-CPT, and P(Cy-S-CPT) at 10 mg/kg CPT-equivalent every three days; (i) Final tumor weights and inhibition rates (IRT) with representative images (*p < 0.1; ***p < 0.001). The above figures are reproduced with permission from references 116 and 117, with authorization for citation.

conjugated to acetylated lysine and polyethylene glycol (Fig. 14e). In its initial state, PLCy is both nonfluorescent and nontoxic, engineered to activate specifically within the tumor microenvironment. The activation process relies on interactions with histone deacetylases (HDACs) and cathepsin L (CTSL), enzymes that are significantly upregulated in cancer cells. These interactions not only

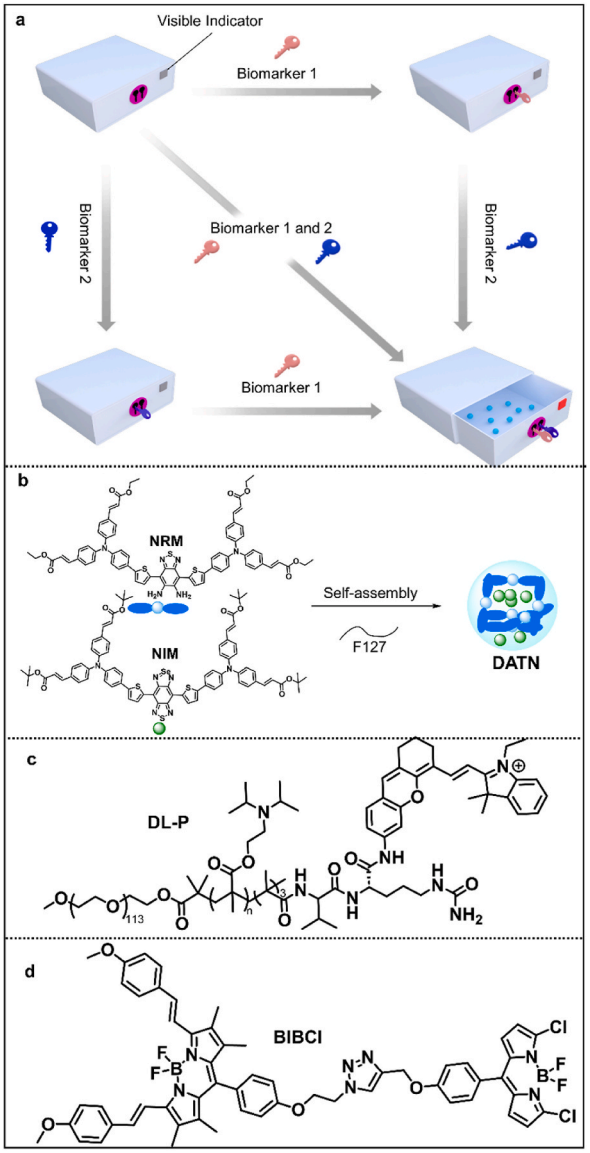

Fig. 16. Dual-key AND-gate probes for integrated tumor diagnosis and treatment. (a) Diagram illustrating a dual-key AND-gate probe activation process. The probe remains inactive with only one biomarker present. However, when both Biomarker 1 and Biomarker 2 are simultaneously present, it triggers not only drug release but also activates a fluorescent signal for real-time monitoring of the therapeutic process; (b) Illustration of the self-assembly process of a nitric oxide-responsive molecule (**NRM**) and a nitric oxide-insensitive molecule (**NIM**) with surfactant F127 to create nanoprobe **DATN**. DATN facilitates cancer imaging and photothermal therapy, activated by dual-key stimuli of nitric oxide (NO) and acidity in tumor environments; (c–d) Structure of AND-logic gate theranostic probes **DL-P** and **BIBCI.**

enable **PLCy**'s mitochondrial targeting but also initiate its therapeutic function. Once activated, **PLCy** markedly diminishes the mitochondrial membrane potential and elevates intracellular ROS levels, resulting in substantial cytotoxic effects on cancer cells. This selective activity was demonstrated in vitro, where **PLCy** exhibited targeted fluorescence activation and cytotoxicity in 4T1 and MCF-7 cancer cells, while sparing normal MEF cells. In vivo validations in a mouse model of breast cancer confirmed the probe's capability to inhibit tumor growth effectively, as evidenced by various tumor analyses and histopathological examinations indicating apoptosis within the treated tumors. This research underscores the potential of leveraging enzyme-responsive activation coupled with mitochondrial targeting to achieve precise imaging and therapeutic outcomes. **PLCy** represents a novel paradigm in macrotheranostic probes, offering targeted, efficient strategies for cancer diagnostics and therapy, and setting a foundation for future advancements in the field.

4.2. AND-logic gate dual-locked probes for tumor theranostics

AND-logic gate dual-locked probes, exemplified by their dual-lock mechanisms, are precisely activated by distinct stimuli in the tumor microenvironment, such as acidity, enzyme overexpression, nitric oxide, and glutathione levels. This selectivity enables accurate imaging and targeted therapy, minimizing effects on healthy cells and maximizing treatment efficacy. These probes, integrating dual-responsive capabilities, ensure precise tumor targeting and enhanced therapeutic results, representing advanced theranostic innovation for personalized medicine (Fig. 16 a).

Building on this concept, a specific example is the development of a dual-stimuli responsive theranostic nanoprobe **DATN** by Zhang et al., designed for accurate cancer imaging and therapy [109]. This nanoprobe incorporates a sophisticated NO/acidity-responsive donor−π-acceptor−π-donor (D−π-A−π-D) molecular structure, paired with a stable reference molecule to ensure consistent performance (Fig. 16b).Upon encountering nitric oxide (NO) within acidic tumor microenvironments, the electron acceptor undergoes oxidation, transforming into a more potent acceptor, 5H- [1,2,3]triazolo [4,5-f]-2,1,3-benzothiadiazole. This transformation facilitates a substantial increase in near-infrared (NIR) absorption via an intramolecular charge transfer mechanism, enhancing the probe's optical properties. Designed with a "dual-key−one-lock" activation mechanism, DATN is finely tuned to respond to the simultaneous presence of NO and acidity, characteristic of the tumor microenvironment. This specific response initiates a photoacoustic signal that allows for targeted in vivo imaging, providing a highly specific visualization of tumor tissues, particularly advantageous for tumors with inflammatory characteristics (Fig. 17a–c). Additionally, DATN is capable of initiating targeted photothermal therapy upon activation, exploiting the combined effects of NO and acidity to enhance its therapeutic photothermal properties for the selective eradication of tumor cells (Fig. 17d–f). Overall, **DATN** represents a cutting-edge theranostic tool, integrating targeted imaging with localized therapeutic action, offering a promising new avenue for more precise and effective cancer treatment strategies.

Building upon this, Yuan et al. introduced an innovative dual-locking nanoprobe **DL-P**, based on hemicyanine, designed to offer enhanced precision in cancer imaging and therapy by responding to orthogonal stimuli [120]. This DL-P nanoprobe incorporates a near-infrared (NIR) hemicyanine dye (CyNH2), linked to a pH-responsive polymer (PEG-b-P(DPA-co-MAA) (Fig. 16 c). This design integrates 2-(diisopropylamino)-ethyl methacrylate (DPA) for sensitivity to lysosomal pH and methacrylic acid (MAA) for conjugation with a CTB-specific dipeptide, valine-citrulline (Val-Cit), introducing a second stimulus-responsive element. The dual-locking mechanism is devised to react to distinct stimuli: acidic pH within lysosomes and the presence of CTB, a cancer-associated biomarker. The first lock's activation by the acidic environment triggers the probe's fluorescence for imaging and initiates therapeutic agent release. The second lock, responsive to Val-Cit cleavage by CTB, further ensures the probe's activation and drug delivery specifically within cancer cells. Upon entry into tumor cells, **DL-P** reacts to the simultaneous presence of acidic pH and elevated CTB levels, leading to **CyNH2** release and significant NIR fluorescence emission, enabling detailed cancer imaging. Concurrently, CyNH2 induces mitochondrial dysfunction, targeting cancer cell viability effectively. In contrast, in normal cells, **CyNH2** fluorescence remains quenched, minimizing toxicity and preserving healthy tissue integrity. This nuanced response to lysosomal pH and CTB overexpression underscores **DL-P**'s specificity and selectivity, making it an exceptional tool for targeted cancer diagnostics and therapeutics, illustrating its potential as a highly precise modality in the emerging realm of cancer theranostics.

Expanding on the concept of targeted activation, Yang et al. developed a "dual lock-and-key" supramolecular photosensitizer named **BIBCl–PAE NPs**, aimed at enhancing the specificity and efficacy of cancer treatment [121]. These nanoparticles encapsulate a glutathione (GSH)-activatable photosensitizer, **BIBCl**, within a pH-responsive diblock copolymer, PEG-b-P(DPA-co-MAA). The photosensitizer comprises an iodine-substituted BODIPY (BI) unit and a chlorine-substituted BODIPY (BCl) unit, as depicted in Fig. 16d. The BI unit's heavy atomic iodine facilitates the generation of singlet oxygen ($^1O_2$) via intersystem crossing (ISC), which is amplified by heavy atom effects and oxygen energy transfer. Additionally, the BCl unit serves both as a GSH-responsive element and a light-harvesting component, enhancing stability in non-target tissues and mitigating aggregation-caused quenching (ACQ). Within normal tissues, the photosensitizer remains inactive due to its aggregated state within the micelle. However, in the tumor-specific environment characterized by acidic pH and elevated GSH levels, the nanoparticles undergo a two-stage activation process. Initially, acidic conditions prompt the disassembly of the micelles, followed by GSH interactions that release BIBSG—a water-soluble photosensitizer with enhanced photodynamic properties. In vitro evaluations have demonstrated the system's capacity to differentiate between cancerous and normal cells, achieving targeted cancer cell ablation while sparing healthy tissues. Subsequent in vivo studies confirmed rapid accumulation of the nanoparticles at tumor sites and their precise activation, leading to localized cytotoxic effects on tumor cells (Fig. 17g and **h**). Mice treated with **BIBH–PAE NPs** or BIBH–PCL NPs showed minimal tumor growth inhibition, supporting the strategy where photosensitizers (PSs) react with GSH in a mildly acidic tumor microenvironment to form water-soluble molecules, reducing ACQ and enhancing PDT efficacy. On the 15th day, differences in therapeutic outcomes were evident from tumor images and average weights, with the BIBCl–PAE NPs light group showing the most significant antitumor effect (Fig. 17i–k).This dual-triggered

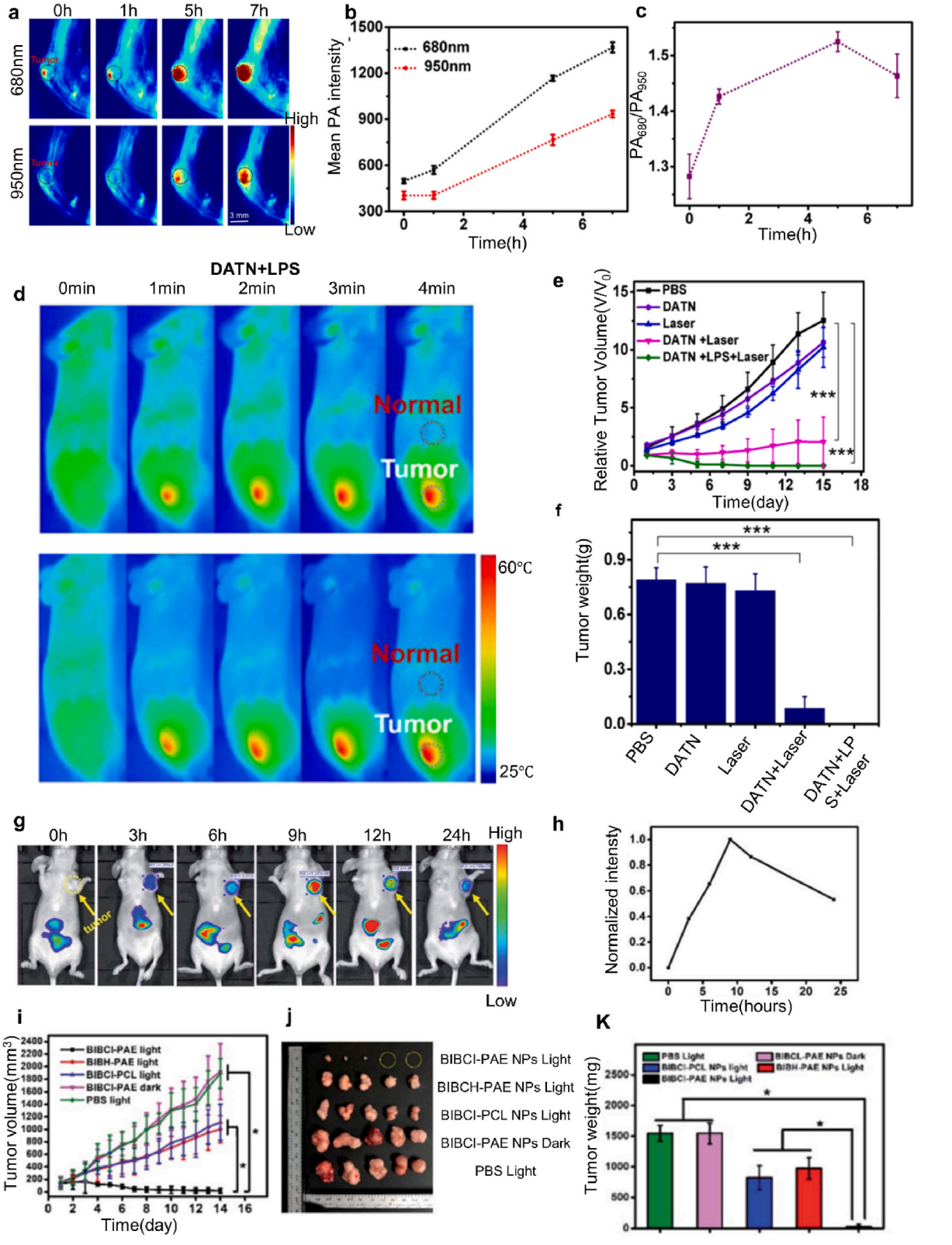

(caption on next page)

Fig. 17. (a) PA images of endogenous NO in 4T1 tumor-bearing mice after DATN injection; (b) Quantified PA signals in tumor regions; (c) PA680/PA950 ratio changes over time; (d) Photothermal images of mice irradiated with 660 nm and 980 nm lasers at 7 h post-injection; (e) Tumor growth curves (***$p < 0.001$); (f) Tumor weights 15 days post-irradiation (***$p < 0.001$); (g) Fluorescence imaging of HepG2 tumor-bearing mice after BIBCl–PAE NPs injection (2 mg/kg BIBCl); (h) Normalized fluorescence intensity at tumor sites over time; (i) Tumor growth profiles during observation; (j) Images of excised tumors from different groups; (k) Average tumor weights across groups. The above figures are reproduced with permission from references 109 and 121, with authorization for citation.

activation system, **BIBCl–PAE NPs**, represents a significant advancement in cancer therapeutics, offering a refined approach that addresses the limitations of conventional photosensitizers and opens new avenues for their clinical application in cancer.

5. Conclusions and outlook

In this review, we have comprehensively explored the advancements in dual-lock probes for tumor diagnostics and therapy. We have elaborated on various design strategies employed to construct these probes, targeting specific tumor microenvironments such as acidity, hypoxia, and viscosity, and responding to bioactive small molecules like hydrogen sulfide, nitric oxide, and hypochlorous acid, as well as tumor-related enzymes including tyrosinase, MMP-2, and cathepsin B. Compared to single-stimulus responsive probes, dual-lock probes excel in reducing non-specific activation and false positives in complex environments. Integrating drug delivery with imaging, these probes exemplify the efficacy of dual-lock systems in enhancing therapeutic outcomes and precision imaging. We foresee that these systems will deepen our understanding of the pharmacological impact during treatment, as demonstrated by probes like P(Cy-s-CPt) activated by two cancer biomarkers, acidity, and GSH, to release the anti-cancer drug CPT [117]. Overall, the distinct advantages of dual-lock probes in tumor diagnosis, monitoring, and treatment indicate their pivotal role in both fundamental biology and translational medicine, offering novel insights and solutions for precise disease diagnosis and therapy.

Although dual-locked fluorescent probes for precise diagnosis and targeted treatment of tumors have made significant progress, they still face several challenges. One key challenge is that the dual-locked fluorescent probes may suffer from signal crosstalk due to the spectral overlap, compromising their selectivity. To address this issue, employing two independent optical channels or combining chemiluminescence with fluorescence techniques can offer more precise biomarker discrimination. Secondly, the majority of dual-locked fluorescent probes emit in the visible or NIR-I range, which is prone to significant autofluorescence interference from surrounding biomolecules and tissues. Future research should focus on developing probes with longer wavelengths, particularly those emitting fluorescence in the near-infrared II region, to enhance their depth and efficiency in in vivo imaging. Thirdly, many of the currently reported dual-locked fluorescent probes lack sufficient sensitivity and specificity, while relevant bioactive molecules within tumor cells typically exist at very low concentrations. Therefore, it is necessary to enhance detection sensitivity for real-time, sensitive monitoring of these bioactive substances within living cells. To improve specificity, a promising approach involves incorporating tumor-specific targeting groups into the probe molecule, such as those that bind to overexpressed receptors like folate or biotin in cancer cells. This enables the probes to accumulate preferentially in cancer cells rather than normal cells. Once inside the cancer cells, the probes can be activated by specific biomarkers, resulting in a fluorescent signal. This strategy not only enhances the signal-to-noise ratio but also improves the accuracy of distinguishing cancer cells from normal cells. The potential for clinical application of dual-lock probes warrants further investigation. To facilitate their integration into clinical research, it is crucial to focus on improving key aspects such as photostability, penetration depth, optimized excitation and emission wavelengths, and biocompatibility. One promising avenue is utilizing dual-lock probes for the analysis of clinical biological samples, including urine and tissue biopsies. This approach could yield more comprehensive insights compared to traditional diagnostic methods like ELISA tests and immunohistochemistry.

Data availability statement

No data was used for the research described in the article.

CRediT authorship contribution statement

Tang Gao: Writing – review & editing, Funding acquisition. **Can Xiang:** Writing – review & editing, Writing – original draft. **Xintao Ding:** Validation. **Mingxing Xie:** Project administration, Conceptualization.

Declaration of competing interest

The authors declare that they have no known competing financial interests or personal relationships that could have appeared to influence the work reported in this paper.

Acknowledgements

This study was supported by the Natural Science Foundation of China (82202234), and the Natural Science Foundation of Hubei (2023AFB753).

References

[1] H. Sung, J. Ferlay, R.L. Siegel, M. Laversanne, I. Soerjomataram, A. Jemal, et al., Global cancer statistics 2020: GLOBOCAN estimates of incidence and mortality worldwide for 36 cancers in 185 countries, CA. Cancer J. Clin. 71 (2021) 209–249.
[2] T. Yoshikawa, N. Ishiwa, S. Morinaga, Y. Noguchi, Y. Yamamoto, Can surgical diagnosis of “early” gastric cancer and lymph node metastasis be accurate? Gastric Cancer 7 (2004) 36–40.
[3] S.J. Henley, E.M. Ward, S. Scott, J. Ma, R.N. Anderson, A.U. Firth, et al., Annual report to the nation on the status of cancer, part I: National cancer statistics, Cancer 126 (2020) 2225–2249.
[4] F. Bray, J. Ferlay, I. Soerjomataram, R.L. Siegel, L.A. Torre, A. Jemal, Global cancer statistics 2018: GLOBOCAN estimates of incidence and mortality worldwide for 36 cancers in 185 countries, CA. Cancer J. Clin. 68 (2018) 394–424.
[5] J. Li, X. Guan, Z. Fan, L.-M. Ching, Y. Li, X. Wang, et al., Non-invasive biomarkers for early detection of breast cancer, Cancers 12 (2020) 2767.
[6] B.A. Webb, M. Chimenti, M.P. Jacobson, D.L. Barber, Dysregulated pH: a perfect storm for cancer progression, Nat. Rev. Cancer 11 (2011) 671–677.
[7] Y. Wang, K. Zhou, G. Huang, C. Hensley, X. Huang, X. Ma, et al., A nanoparticle-based strategy for the imaging of a broad range of tumours by nonlinear amplification of microenvironment signals, Nat. Mater. 13 (2014) 204–212.
[8] H. Kobayashi, M. Ogawa, R. Alford, P.L. Choyke, Y. Urano, New strategies for fluorescent probe design in medical diagnostic imaging, Chem. Rev. 110 (2010) 2620–2640.
[9] A.L. Vahrmeijer, M. Hutteman, J.R. Van Der Vorst, C.J. Van De Velde, J.V. Frangioni, Image-guided cancer surgery using near-infrared fluorescence, Nat. Rev. Clin. Oncol. 10 (2013) 507–518.
[10] H. Li, H. Kim, F. Xu, J. Han, Q. Yao, J. Wang, et al., Activity-based NIR fluorescent probes based on the versatile hemicyanine scaffold: design strategy, biomedical applications, and outlook, Chem. Soc. Rev. 51 (2022) 1795–1835.
[11] A.P. De Silva, H.N. Gunaratne, T. Gunnlaugsson, A.J. Huxley, C.P. McCoy, J.T. Rademacher, et al., Signaling recognition events with fluorescent sensors and switches, Chem. Rev. 97 (1997) 1515–1566.
[12] H.-W. Liu, L. Chen, C. Xu, Z. Li, H. Zhang, X.-B. Zhang, et al., Recent progresses in small-molecule enzymatic fluorescent probes for cancer imaging, Chem. Soc. Rev. 47 (2018) 7140–7180.
[13] K. Wang, C. Liu, H. Zhu, Y. Zhang, M. Su, X. Wang, et al., Recent advances in small-molecule fluorescent probes for diagnosis of cancer cells/tissues, Coord. Chem. Rev. 477 (2023) 214946.
[14] Y. Li, C. Xue, Z. Fang, W. Xu, H. Xie, In vivo visualization of γ-Glutamyl transpeptidase activity with an activatable self-immobilizing near-infrared probe, Anal. Chem. 92 (2020) 15017–15024.
[15] H. Zhang, J. Liu, C. Liu, P. Yu, M. Sun, X. Yan, et al., Imaging lysosomal highly reactive oxygen species and lighting up cancer cells and tumors enabled by a Si-rhodamine-based near-infrared fluorescent probe, Biomaterials 133 (2017) 60–69.
[16] T. Zhang, F. Huo, W. Zhang, J. Chao, C. Yin, Ultra-pH-sensitive sensor for visualization of lysosomal autophagy, drug-induced pH alteration and malignant tumors microenvironment, Sens. Actuators B. Chem. 345 (2021) 130393.
[17] M. Bertolini, M.S. Wong, L. Mendive-Tapia, M. Vendrell, Smart probes for optical imaging of T cells and screening of anti-cancer immunotherapies, Chem. Soc. Rev. 52 (2023) 5352–5372.
[18] M. Gao, F. Yu, C. Lv, J. Choo, L. Chen, Fluorescent chemical probes for accurate tumor diagnosis and targeting therapy, Chem. Soc. Rev. 46 (2017) 2237–2271.
[19] K. Wang, Y. Du, Z. Zhang, K. He, Z. Cheng, L. Yin, et al., Fluorescence image-guided tumour surgery, Nat. Rev. Bioeng. 1 (2023) 161–179.
[20] L. Wu, J. Huang, K. Pu, T.D. James, Dual-locked spectroscopic probes for sensing and therapy, Nat. Rev. Chem 5 (2021) 406–421.
[21] A. Romieu, "AND" luminescent "reactive" molecular logic gates: a gateway to multi-analyte bioimaging and biosensing, Org. Biomol. Chem. 13 (2015) 1294–1306.
[22] H. Feng, Q. Meng, H.T. Ta, R. Zhang, Development of “dual-key-and-lock” responsive probes for biosensing and imaging, New J. Chem. 44 (2020) 12890–12896.
[23] Y.-L. Qi, L.-L. Chen, L. Guo, Y.-Y. Cao, H.-R. Wang, Y.-S. Yang, et al., Multifunctional fluorescent probes "killing two birds with one stone" - recent progress and outlook, Appl. Mater. Today 21 (2020) 100877.
[24] C. Yu, D. Wu, L. Dai, X. He, J.-T. Hou, J. Shen, et al., Fluorescent sensors for discriminative detection of multiple targets in pathological processes, Coord. Chem. Rev. 489 (2023) 215203.
[25] J. Guo, B. Fang, H. Bai, L. Wang, B. Peng, X.-J. Qin, et al., Dual/Multi-responsive fluorogenic probes for multiple analytes in mitochondria: from design to applications, TrAC. Trends Anal. Chem. (2022) 116697.
[26] G. Blum, G. Von Degenfeld, M.J. Merchant, H.M. Blau, M. Bogyo, Noninvasive optical imaging of cysteine protease activity using fluorescently quenched activity-based probes, Nat. Chem. Biol. 3 (2007) 668–677.
[27] C.A. Borrebaeck, Precision diagnostics: moving towards protein biomarker signatures of clinical utility in cancer, Nat. Rev. Cancer 17 (2017) 199–204.
[28] J.D. Cohen, L. Li, Y. Wang, C. Thoburn, B. Afsari, L. Danilova, et al., Detection and localization of surgically resectable cancers with a multi-analyte blood test, Science 359 (2018) 926–930.
[29] L. Liu, T. Li, S. Zhang, P. Song, B. Guo, Y. Zhao, et al., Simultaneous quantification of multiple cancer biomarkers in blood samples through DNA-assisted nanopore sensing, Angew Chem. Int. Ed. Engl. 57 (2018) 11882–11887.
[30] J.D. Wulfkuhle, L.A. Liotta, E.F. Petricoin, Proteomic applications for the early detection of cancer, Nat. Rev. Cancer 3 (2003) 267–275.
[31] P.A. Schornack, R.J. Gillies, Contributions of cell metabolism and H+ diffusion to the acidic pH of tumors, Neoplasia 5 (2003) 135–145.
[32] J.W. Wojtkowiak, J.M. Rothberg, V. Kumar, K.J. Schramm, E. Haller, J.B. Proemsey, et al., Chronic autophagy is a cellular adaptation to tumor acidic pH microenvironments, Cancer Res. 2 (2012) 3938–3947.
[33] S. Zhou, L. Jiang, C. Li, H. Mao, C. Jiang, Z. Wang, et al., Acid and hypoxia tandem-activatable deep near-infrared nanoprobe for two-step signal amplification and early detection of cancer, Adv. Mater. (2023) 2212231.
[34] R. Lebel, M. Lepage, A comprehensive review on controls in molecular imaging: lessons from MMP-2 imaging, Contrast Media Mol. Imaging 9 (2014) 187–210.
[35] A. Tanaka, Y. Fukuoka, Y. Morimoto, T. Honjo, D. Koda, M. Goto, et al., Cancer cell death induced by the intracellular self-assembly of an enzyme-responsive supramolecular gelator, J. Am. Chem. Soc. 137 (2015) 770–775.
[36] S.J. Riedl, Y. Shi, Molecular mechanisms of caspase regulation during apoptosis, Nat. Rev. Mol. Cell Biol. 5 (2004) 897–907.
[37] S.-Y. Li, L.-H. Liu, H. Cheng, B. Li, W.-X. Qiu, X.-Z. Zhang, A dual-FRET-based fluorescence probe for the sequential detection of MMP-2 and caspase-3, Chem. Commun. 51 (2015) 14520–14523.
[38] Y. Yuan, C.-J. Zhang, R.T. Kwok, D. Mao, B.Z. Tang, B. Liu, Light-up probe based on AIEgens: dual signal turn-on for caspase cascade activation monitoring, Chem. Sci. 8 (2017) 2723–2728.
[39] I. Mellman, G. Coukos, G. Dranoff, Cancer immunotherapy comes of age, Nature 480 (2011) 480–489.
[40] A. Ribas, J.D. Wolchok, Cancer immunotherapy using checkpoint blockade, Science 359 (2018) 1350–1355.
[41] L.H. Calabrese, C. Calabrese, L.C. Cappelli, Rheumatic immune-related adverse events from cancer immunotherapy, Nat. Rev. Rheumatol. 14 (2018) 569–579.
[42] K. Esfahani, A. Elkrief, C. Calabrese, R. Lapointe, M. Hudson, B. Routy, et al., Moving towards personalized treatments of immune-related adverse events, Nat. Rev. Clin. Oncol. 17 (2020) 504–515.
[43] P. Cheng, S. He, C. Zhang, J. Liu, K. Pu, A tandem-locked fluorescent netosis reporter for the prognosis assessment of cancer immunotherapy, Angew. Chem. Int. Ed. Engl. 26 (2023) e202301625.
[44] X.Z. Wang, S.S. He, P.H. Cheng, K.Y. Pu, A dual-locked tandem fluorescent probe for imaging of pyroptosis in cancer chemo-immunotherapy, Adv. Mater. 10 (2023) 2206510.
[45] S.A. D'Mello, G.J. Finlay, B.C. Baguley, M.E. Askarian-Amiri, Signaling pathways in melanogenesis, Int. J. Mol. Sci. 17 (2016) 1144.
[46] T.P. Szatrowski, C.F. Nathan, Production of large amounts of hydrogen peroxide by human tumor cells, Cancer Res. 51 (1991) 794–798.

[47] H.Y. Peng, T. Wang, G.R. Li, J. Huang, Q. Yuan, Dual-locked near-infrared fluorescent probes for precise detection of melanoma via hydrogen peroxide-tyrosinase cascade activation, Anal. Chem. 94 (2022) 1070–1075.
[48] T. Almammadov, M. Dirak, A. Saymaz, A. Acari, S. Kolemen, A hydrogen sulfide and tyrosinase responsive dual-locked fluorophore for selective imaging of melanoma cells, Chem.Commun. 59 (2023) 9972–9975.
[49] R. Wang, K. Yin, M. Ma, T. Zhu, J. Gao, J. Sun, et al., Alkaline phosphatase-initiated sensitive responsiveness of activatable probes to hydrogen sulfide for accurate cancer imaging and differentiation, CCS Chem. 4 (2022) 3715–3723.
[50] S. Evans, R. Lew, M. Kochman, E. Wileyto, E. Baum, K. Safford, et al., Human esophageal cancer is distinguished from adjacent esophageal tissue by tissue cysteine concentrations, Dig. Dis. Sci. 47 (2002) 2743–2750.
[51] M.G. Vander Heiden, L.C. Cantley, C.B. Thompson, Understanding the Warburg effect: the metabolic requirements of cell proliferation, Science 324 (2009) 1029–1033.
[52] C. Szabo, C. Coletta, C. Chao, K. Módis, B. Szczesny, A. Papapetropoulos, et al., Tumor-derived hydrogen sulfide, produced by cystathionine-β-synthase, stimulates bioenergetics, cell proliferation, and angiogenesis in colon cancer, P Proc. Natl. Acad. Sci. USA. 110 (2013) 12474–12479.
[53] Z.-P. She, W.-X. Wang, G.-J. Mao, W.-L. Jiang, Z.-Q. Wang, Y. Li, et al., A near-infrared fluorescent probe for accurately diagnosing cancer by sequential detection of cysteine and H^+, Chem. Commun. 57 (2021) 4811–4814.
[54] Z.-P. She, W.-X. Wang, W.-L. Jiang, Z.-Q. Wang, G.-J. Mao, J. Fei, et al., Accurate fluorescence diagnosis of cancer based on sequential detection of hydrogen sulfide and pH, Anal. Chem. 93 (2021) 11826–11835.
[55] H.A. Lardy, S.M. Ferguson, Oxidative phosphorylation in mitochondria, Annu. Rev. Biochem. 38 (1969) 991–1034.
[56] P.G. Finichiu, A.M. James, L. Larsen, R.A. Smith, M.P. Murphy, Mitochondrial accumulation of a lipophilic cation conjugated to an ionisable group depends on membrane potential, pH gradient and pK a: implications for the design of mitochondrial probes and therapies, J. Bioenerg. Biomembr. 45 (2013) 165–173.
[57] L.B. Chen, Mitochondrial membrane potential in living cells, Annu. Rev. Cell Biol. 4 (1988) 155–181.
[58] J.S. Modica-Napolitano, J.R. Aprille, Delocalized lipophilic cations selectively target the mitochondria of carcinoma cells, Adv. Drug Deliv. Rev. 49 (2001) 63–70.
[59] Y. Shi, S.K. Lim, Q. Liang, S.V. Iyer, H.-Y. Wang, Z. Wang, et al., Gboxin is an oxidative phosphorylation inhibitor that targets glioblastoma, Nature 567 (2019) 341–346.
[60] N. Jiang, J. Fan, F. Xu, X. Peng, H. Mu, J. Wang, et al., Ratiometric fluorescence imaging of cellular polarity: decrease in mitochondrial polarity in cancer cells, Angew Chem. Int. Ed. Engl. 54 (2015) 2510–2514.
[61] P.E. Klier, J.G. Martin, E.W. Miller, Imaging reversible mitochondrial membrane potential dynamics with a masked rhodamine voltage reporter, J. Am. Chem. Soc. 143 (2021) 4095–4099.
[62] M. Zhao, J. Wang, Z. Lei, L. Lu, S. Wang, H. Zhang, et al., NIR-II pH sensor with a FRET adjustable transition point for in situ dynamic tumor microenvironment visualization, Angew Chem. Int. Ed. Engl. 133 (2021) 5151–5155.
[63] Z. Liang, Y. Sun, R. Duan, R. Yang, L. Qu, K. Zhang, et al., Low polarity-triggered basic hydrolysis of coumarin as an AND logic gate for broad-spectrum cancer diagnosis, Anal. Chem. 93 (2021) 12434–12440.
[64] M.-C. Hung, G.B. Mills, D. Yu, Oxygen sensor boosts growth factor signaling, Nat. Med. 15 (2009) 246–247.
[65] X. Cui, L. Li, G. Yan, K. Meng, Z. Lin, Y. Nan, et al., High expression of NQO1 is associated with poor prognosis in serous ovarian carcinoma, BMC Cancer 15 (2015) 1–8.
[66] F. Kong, Y. Li, C. Yang, X. Li, J. Wu, X. Liu, et al., A fluorescent probe for simultaneously sensing NTR and hNQO1 and distinguishing cancer cells, J. Mater. Chem. B 7 (2019) 6822–6827.
[67] J.C. Widen, M. Tholen, J.J. Yim, A. Antaris, K.M. Casey, S. Rogalla, et al., AND-gate contrast agents for enhanced fluorescence-guided surgery, Nat. Biomed. Eng. 5 (2021) 264–277.
[68] C. Zhang, Q.Z. Zhang, K. Zhang, L.Y. Li, M.D. Pluth, L. Yi, et al., Dual-biomarker-triggered fluorescence probes for differentiating cancer cells and revealing synergistic antioxidant effects under oxidative stress, Chem. Sci. 10 (2019) 1945–1952.
[69] C. Wang, Y. Hong, L. Dong, H. Cheng, D. Jin, R. Zhao, et al., An AND-gate bioluminescent probe for precise tumor imaging, Chem. Sci. 14 (2023) 5768–5773.
[70] L.B. Pontel, I.V. Rosado, G. Burgos-Barragan, J.I. Garaycoechea, R. Yu, M.J. Arends, et al., Endogenous formaldehyde is a hematopoietic stem cell genotoxin and metabolic carcinogen, Mol. Cell 60 (2015) 177–188.
[71] Y. Lai, R. Yu, H.J. Hartwell, B.C. Moeller, W.M. Bodnar, J.A. Swenberg, Measurement of endogenous versus exogenous formaldehyde-induced DNA-protein crosslinks in animal tissues by stable isotope labeling and ultrasensitive mass spectrometry, Cancer Res. 76 (2016) 2652–2661.
[72] Z. Tong, W. Luo, Y. Wang, F. Yang, Y. Han, H. Li, et al., Tumor tissue-derived formaldehyde and acidic microenvironment synergistically induce bone cancer pain, PLoS One 5 (2010) e10234.
[73] C. Liu, R. Zhang, W. Zhang, J. Liu, Y.-L. Wang, Z. Du, et al., "Dual-key-and-lock" ruthenium complex probe for lysosomal formaldehyde in cancer cells and tumors, J. Am. Chem. Soc. 141 (2019) 8462–8472.
[74] X. Du, X. Fu, K. Yao, Z. Lan, H. Xu, Q. Cui, et al., Bcl-2 delays cell cycle through mitochondrial ATP and ROS, Cell Cycle 16 (2017) 707–713.
[75] Y. Kato, S. Ozawa, C. Miyamoto, Y. Maehata, A. Suzuki, T. Maeda, et al., Acidic extracellular microenvironment and cancer, Cancer Cell Int. 13 (2013) 1–8.
[76] T.W. Traut, Physiological concentrations of purines and pyrimidines, Mol. Cell. Biochem. 140 (1994) 1–22.
[77] Y.W. Jun, K.H. Kim, Y.J. Yang, Y. Jung, K.-T. Kim, H. Kim, et al., Discrimination of invasive human skin tumor using an ultrafast ATP–proton AND-gate probe, ACS Sens. 7 (2022) 1068–1074.
[78] X. Liu, X. Gong, J. Yuan, X. Fan, X. Zhang, T. Ren, et al., Dual-stimulus responsive near-infrared reversible ratiometric fluorescent and photoacoustic probe for in vivo tumor imaging, Anal. Chem. 93 (2021) 5420–5429.
[79] K. Dou, C. Fan, W.Q. Feng, Y. Kong, Y.H. Xiang, Z.J. Wang, et al., "Dual-Lock-Dual-Key" controlled second near-infrared molecular probe for specific discrimination of orthotopic colon cancer and imaging-guided tumor excision, CCS Chem. 4 (2022) 3609–3626.
[80] W. Huo, K. Miki, D. Tokunaga, H. Mu, M. Oe, H. Harada, et al., Dual-stimuli-responsive probes for detection of ovarian cancer cells and quantification of both ph and enzyme activity, Bull. Chem. Soc. Jpn. 94 (2021) 2068–2075.
[81] A. Fernandez, E.J. Thompson, J.W. Pollard, T. Kitamura, M. Vendrell, A fluorescent activatable AND-Gate chemokine CCL2 enables in vivo detection of metastasis-associated macrophages, Angew. Chem. Int. Ed. Engl. 58 (2019) 16894–16898.
[82] S. Stöcker, M. Maurer, T. Ruppert, T.P. Dick, A role for 2-Cys peroxiredoxins in facilitating cytosolic protein thiol oxidation, Nat. Chem. Biol. 14 (2018) 148–155.
[83] P.D. Ray, B.-W. Huang, Y. Tsuji, Reactive oxygen species (ROS) homeostasis and redox regulation in cellular signaling, Cell. Signal. 24 (2012) 981–990.
[84] Y. Chen, J.-Y. Lim, X.H. Wu, J.S. Heo, J.F. Zhang, D.W. Yoon, et al., Development of H_2S and HClO dual-responsive fluorescent probe for cancer recognition, Dyes Pigm (2021) 109666.
[85] Z. Jiang, W. Wang, G. Perry, X. Zhu, X. Wang, Mitochondrial dynamic abnormalities in amyotrophic lateral sclerosis, Transl. Neurodegener. 4 (2015) 1–6.
[86] D.A. Erlanson, S.W. Fesik, R.E. Hubbard, W. Jahnke, H. Jhoti, Twenty years on: the impact of fragments on drug discovery, Nat. Rev. Drug Discov. 15 (2016) 605–619.
[87] C.C. Winterbourn, M.B. Hampton, J.H. Livesey, A.J. Kettle, Modeling the reactions of superoxide and myeloperoxidase in the neutrophil phagosome: implications for microbial killing, J. Biol. Chem. 281 (2006) 39860–39869.
[88] M. Visscher, M.R. Arkin, T.B. Dansen, Covalent targeting of acquired cysteines in cancer, Curr. Opin. Chem. Biol. 30 (2016) 61–67.
[89] N. Zhu, X. Guo, S. Pang, Y. Chang, X. Liu, Z. Shi, et al., Mitochondria-immobilized unimolecular fluorescent probe for multiplexing imaging of living cancer cells, Anal. Chem. 92 (2020) 11103–11110.
[90] X. Yang, J. Liu, P. Xie, X. Han, D. Zhang, Y. Ye, et al., Visualization of biothiols and HClO in cancer therapy via a multi-responsive fluorescent probe, Sens Actuators B. Chem. 347 (2021) 130620.

[91] H. Cheng, S.-Y. Li, H.-R. Zheng, C.-X. Li, B.-R. Xie, K.-W. Chen, et al., Multi-forster resonance energy transfer-based fluorescent probe for spatiotemporal matrix metalloproteinase-2 and caspase-3 imaging, Anal. Chem. 89 (2017) 4349–4354.
[92] A. Megia-Fernandez, B. Mills, C. Michels, S.V. Chankeshwara, N. Krstajić, C. Haslett, et al., Bimodal fluorogenic sensing of matrix proteolytic signatures in lung cancer, Org. Biomol. Chem. 16 (2018) 8056–8063.
[93] M. Yasukawa, H. Ohminami, J. Arai, Y. Kasahara, Y. Ishida, S. Fujita, Granule exocytosis, and not the Fas/Fas ligand system, is the main pathway of cytotoxicity mediated by alloantigen-specific $CD4^+$ as well as $CD8^+$ cytotoxic T lymphocytes in humans, Blood 95 (2000) 2352–2355.
[94] S. Cullen, S. Martin, Mechanisms of granule-dependent killing, Cell Death Dis. 15 (2008) 251–262.
[95] M. Li, J. Tang, C. Lin, A. Shen, X. Ma, J. Wu, et al., A smart responsive fluorescence-mr nanoprobe for monitoring tumor response to immunotherapy, Adv. Healthc. Mater. (2023) 2300602.
[96] J. Yin, L. Huang, L. Wu, J. Li, T.D. James, W. Lin, Small molecule based fluorescent chemosensors for imaging the microenvironment within specific cellular regions, Chem. Soc. Rev. 50 (2021) 12098–12150.
[97] Z. Yang, J. Cao, Y. He, J.H. Yang, T. Kim, X. Peng, et al., Macro-/micro-environment-sensitive chemosensing and biological imaging, Chem. Soc. Rev. 43 (2014) 4563–4601.
[98] L. Yang, P. Gu, A. Fu, Y. Xi, S. Cui, L. Ji, et al., TPE-based fluorescent probe for dual channel imaging of pH/viscosity and selective visualization of cancer cells and tissues, Talanta (2023) 124862.
[99] Y. Fang, W. Shi, Y. Hu, X. Li, H. Ma, A dual-function fluorescent probe for monitoring the degrees of hypoxia in living cells via the imaging of nitroreductase and adenosine triphosphate, Chem. Commun. 54 (2018) 5454–5457.
[100] G.-Y. Liou, P. Storz, Reactive oxygen species in cancer, Free Radic. Res. 44 (2010) 479–496.
[101] S. Galadari, A. Rahman, S. Pallichankandy, F. Thayyullathil, Reactive oxygen species and cancer paradox: to promote or to suppress? Free Radic. Biol. Med. 104 (2017) 144–164.
[102] Y. Wen, F. Huo, J. Wang, C. Yin, Multicolor fluorescence based on FRET regulated by functional peptides to screen high metastatic potential cancer cells, Anal. Chem. 91 (2019) 15057–15063.
[103] P. Guan, S. Shi, T. Zhang, J. Chai, B. Yang, B. Liu, A strategy to distinguish cancers from normal cells through lysosomal targeted double site fluorescent probe for lipase and hydrogen sulfide, Dyes Pigm. 205 (2022) 110545.
[104] J. Rautio, N.A. Meanwell, L. Di, M.J. Hageman, The expanding role of prodrugs in contemporary drug design and development, Nat. Rev. Drug Discov. 17 (2018) 559–587.
[105] L. Bildstein, C. Dubernet, P. Couvreur, Prodrug-based intracellular delivery of anticancer agents, Adv. Drug Deliv. Rev. 63 (2011) 3–23.
[106] J.L. Kolanowski, F. Liu, E.J. New, Fluorescent probes for the simultaneous detection of multiple analytes in biology, Chem. Soc. Rev. 47 (2018) 195–208.
[107] S. Wang, G. Yu, Z. Wang, O. Jacobson, L.S. Lin, W. Yang, et al., Enhanced antitumor efficacy by a cascade of reactive oxygen species generation and drug release, Angew. Chem. Int. Ed. Engl. 131 (2019) 14900–14905.
[108] S. Biswas, Y. Rajesh, S. Barman, M. Bera, A. Paul, M. Mandal, et al., A dual-analyte probe: hypoxia activated nitric oxide detection with phototriggered drug release ability, Chem. Commun. 54 (2018) 7940–7943.
[109] L. Teng, G. Song, Y. Liu, X. Han, Z. Li, Y. Wang, et al., Nitric oxide-activated "dual-key–one-lock" nanoprobe for in vivo molecular imaging and high-specificity cancer therapy, J. Am. Chem. Soc. 141 (2019) 13572–13581.
[110] G. Li, Y. Yang, Y. Zhang, P. Huang, J. Yan, Z. Song, et al., A reactive oxygen species-tyrosinase cascade-activated prodrug for selectively suppressing melanoma, CCS Chem. 4 (2022) 1654–1670.
[111] Z. Lu, G. Xu, X. Yang, S. Liu, Y. Sun, L. Chen, et al., Dual-activated nano-prodrug for chemo-photodynamic combination therapy of breast cancer, Int. J. Mol. Sci. 23 (2022) 15656.
[112] L.K. Tam, L. Yu, R.C. Wong, W.-P. Fong, D.K. Ng, P.-C. Lo, Dual cathepsin B and glutathione-activated dimeric and trimeric phthalocyanine-based photodynamic molecular beacons for targeted photodynamic therapy, J. Med. Chem. 64 (2021) 17455–17467.
[113] L.K. Tam, L. He, D.K. Ng, P.C. Cheung, P.C. Lo, A tumor-targeting dual-stimuli-activatable photodynamic molecular beacon for precise photodynamic therapy, Chem. Eur J. 28 (2022) e202201652.
[114] L.K. Tam, J.C. Chu, L. He, C. Yang, K.-C. Han, P.C.K. Cheung, et al., Enzyme-responsive double-locked photodynamic molecular beacon for targeted photodynamic anticancer therapy, J. Am. Chem. Soc. 145 (2023) 7361–7375.
[115] M. Chen, C. Wang, X. Wang, Z. Tu, Z. Ding, Z. Liu, An "AND" logic-gated prodrug micelle locally stimulates antitumor immunity, Adv. Mater. 36 (2024) 2307818.
[116] W.X. Wang, J.J. Chao, Z.Q. Wang, T. Liu, G.J. Mao, B. Yang, et al., Dual key-activated NIR-I/II fluorescence probe for monitoring photodynamic and photothermal synergistic therapy efficacy, Adv. Healthc. Mater. 12 (2023) 2301230.
[117] C. Yan, Z. Guo, Y. Liu, P. Shi, H. Tian, W.-H. Zhu, A sequence-activated AND logic dual-channel fluorescent probe for tracking programmable drug release, Chem. Sci. 9 (2018) 6176–6182.
[118] H. Han, W. Teng, T. Chen, J. Zhao, Q. Jin, Z. Qin, et al., A cascade enzymatic reaction activatable gemcitabine prodrug with an AIE-based intracellular light-up apoptotic probe for in situ self-therapeutic monitoring, Chem.Commun. 53 (2017) 9214–9217.
[119] D. Ma, Q. Zong, Y. Du, F. Yu, X. Xiao, R. Sun, et al., Sequential enzyme-activated macrotheranostic probe for selective tumor mitochondria targeting, Acta Biomater. 135 (2021) 628–637.
[120] Q. Zong, R. Zheng, X. Xiao, M. Jiang, J. Li, Y. Yuan, Dual-locking nanoprobe based on hemicyanine for orthogonal stimuli-triggered precise cancer imaging and therapy, J. Control Release 338 (2021) 307–315.
[121] K.-X. Teng, L.-Y. Niu, Y.-F. Kang, Q.-Z. Yang, Rational design of a "dual lock-and-key" supramolecular photosensitizer based on aromatic nucleophilic substitution for specific and enhanced photodynamic therapy, Chem. Sci. 11 (2020) 9703–9711.